ER Proteostasis Regulators Reduce Amyloidogenic Light Chain Secretion Through an On-Target, ATF6-Independent Mechanism

Bibiana Rius[1], Jaleh S. Mesgarzadeh[1], Isabelle C. Romine[1], Ryan J. Paxman[2], Jeffery W. Kelly[2,3], and R. Luke Wiseman[1,*]

[1]Department of Molecular Medicine, The Scripps Research Institute, La Jolla, CA 92037, [2]Department of Chemistry, The Scripps Research Institute, La Jolla, CA 92037, [3]The Skaggs Institute for Chemical Biology, The Scripps Research Institute, La Jolla, CA 92037

*Corresponding Author:
R. Luke Wiseman
Department of Molecular Medicine
The Scripps Research Institute
La Jolla, CA 92037
Email: wiseman@scripps.edu
Phone: (858) 784-8820

Running Title: ER proteostasis regulators reduce LC secretion independent of ATF6

Keywords: Activating transcription factor 6 (ATF6); ER proteostasis; systemic amyloid disease

SUMMARY

The plasma cell secretion and toxic aggregation of amyloidogenic immunoglobulin light chains (LCs) causes proteotoxicity in Light Chain Amyloidosis (AL). We recently identified endoplasmic reticulum (ER) proteostasis regulators such as compound **147** that reduce secretion and aggregation of LCs implicated in AL (Plate, Cooley et al., 2016). Compound **147** promotes adaptive ER proteostasis remodeling through a mechanism involving covalent modification of multiple protein disulfide isomerases (PDIs) and subsequent activation of the ATF6 unfolded protein response (UPR) -associated transcriptional signaling pathway (Paxman, Plate et al., 2018). Here, we show that the **147**-dependent reduction in amyloidogenic LC secretion from AL patient plasma cells is independent of ATF6 activation, but instead requires on-target PDI modification. Our results reveal pharmacologic targeting of PDIs as a potential strategy to ameliorate AL-associated proteotoxicity and demonstrate that **147** can influence ER proteostasis through multiple on-target mechanisms including ATF6 activation and PDI modification.

IMPACT STATEMENT

This study demonstrates the broad potential for endoplasmic reticulum proteostasis regulator compounds such as **147** to influence secretory proteostasis of disease-associated proteins through multiple on target mechanisms.

41 **INTRODUCTION**

42 Light chain amyloidosis (AL) is the most common systemic amyloid disease, affecting 8-10 people per million
43 per year (Badar, D'Souza et al., 2018, Blancas-Mejia & Ramirez-Alvarado, 2013, Cohen & Comenzo, 2010,
44 Merlini, Comenzo et al., 2014, Merlini, Dispenzieri et al., 2018). AL pathogenesis involves the toxic
45 extracellular aggregation of an amyloidogenic immunoglobulin light chain (LC) that is secreted from a clonally
46 expanded cancerous plasma cell. These LC aggregates deposit on post-mitotic tissues including the heart and
47 kidneys causing organ failure and ultimately death (Badar et al., 2018, Blancas-Mejia, Misra et al., 2018,
48 Brenner, Jain et al., 2004, Diomede, Romeo et al., 2017, Guan, Mishra et al., 2015, Guan, Mishra et al., 2013,
49 Imperlini, Gnecchi et al., 2017, Merlini et al., 2014, Merlini et al., 2018, Shi, Guan et al., 2010). Current
50 treatments for AL use chemotherapy combined with autologous stem cell replacement to eliminate the AL-
51 associated plasma cells (Badar et al., 2018, Gertz, 2018, Kastritis, Dialoupi et al., 2019, Manwani, Hegenbart
52 et al., 2018, Merlini et al., 2018, Milani, Palladini et al., 2018, Pinney, Smith et al., 2013). This reduces
53 circulating serum populations of amyloidogenic LCs, decreasing toxic LC aggregation, promoting clearance of
54 deposited amyloid, and improving organ function (Dember, Sanchorawala et al., 2001, Meier-Ewert,
55 Sanchorawala et al., 2011, Merlini et al., 2018, Salinaro, Meier-Ewert et al., 2017). However, ~30% of AL
56 patients presenting with severe cardiac or renal LC proteotoxicity are too ill at diagnosis to tolerate
57 chemotherapy (Merlini et al., 2018, Palladini, Hegenbart et al., 2014, Wechalekar, Schonland et al., 2013).
58 Thus, new strategies are required to alleviate the LC proteotoxicity on distal tissues and allow
59 chemotherapeutic access to AL patients with severe organ involvement.

60 One strategy to reduce the secretion and toxic aggregation of amyloidogenic proteins is through the
61 adaptive remodeling of the ER proteostasis network comprising ER chaperones (e.g., BiP), folding enzymes
62 (e.g., protein disulfide isomerases, PDIs), and degradation factors (Plate & Wiseman, 2017, Powers, Morimoto
63 et al., 2009). These ER proteostasis pathways function to partition ER proteins between folding, trafficking, and
64 degradation in a process termed ER quality control (Braakman & Bulleid, 2011, Plate & Wiseman, 2017, Sun &
65 Brodsky, 2019). Through this partitioning, ER proteostasis pathways reduce the secretion and aggregation of
66 non-native, aggregation-prone proteins in secretory environments including the ER and extracellular space. In
67 the context of AL, destabilized amyloidogenic LCs escape plasma cell ER quality control, allowing their efficient
68 secretion to the serum (Blancas-Mejia et al., 2018, Eisele, Monteiro et al., 2015, Plate & Wiseman, 2017). This

69 increases extracellular populations of amyloidogenic LCs available for concentration-dependent aggregation
70 into the toxic oligomers and amyloid fibrils implicated in AL pathogenesis.

71 Enhancing ER proteostasis through mechanisms such as activation of the unfolded protein response
72 (UPR)-associated transcription factor ATF6 can selectively reduce the secretion and toxic aggregation of
73 destabilized, amyloidogenic proteins (Kelly, 2020, Plate & Wiseman, 2017). ATF6 induces the expression of
74 many ER proteostasis factors including the ATP-dependent ER HSP70 BiP and multiple protein disulfide
75 isomerases (PDIs) (Haze, Yoshida et al., 1999, Shoulders, Ryno et al., 2013). Genetic activation of ATF6 using
76 a ligand-regulated system preferentially reduces secretion and subsequent aggregation of a destabilized,
77 amyloidogenic LC from HEK293T cells, without impacting the secretion of a non-amyloidogenic LC, fully-
78 assembled IgGs, or the endogenous secretory proteome (Cooley, Ryno et al., 2014, Plate, Rius et al., 2019,
79 Shoulders et al., 2013). Interestingly, the ATF6-dependent reduction in amyloidogenic LC secretion results
80 from increased interactions with ER chaperones and PDIs, which preferentially retain the amyloidogenic LC
81 within the ER and prevent its secretion to downstream secretory environments (Plate et al., 2019). This
82 indicates that pharmacologic approaches that similarly target ER proteostasis could also reduce secretion and
83 toxic aggregation of amyloidogenic LCs implicated in AL (Kelly, 2020, Plate & Wiseman, 2017).

84 Recently, we used high-throughput screening to identify small molecule ER proteostasis regulators that
85 selectively activate the ATF6 UPR signaling pathway (Plate et al., 2016). One of the most promising small
86 molecules emerging from this screen was compound **147**. Using a combination of medicinal chemistry and
87 chemical biology, we showed that **147** activates ATF6 through a mechanism involving compound metabolic
88 activation and covalent labeling of multiple PDIs (Paxman et al., 2018). Since PDIs are involved in regulating
89 the proper folding and disulfide bond formation for ER-targeted proteins (Appenzeller-Herzog & Ellgaard, 2008,
90 Braakman & Bulleid, 2011, Wang, Wang et al., 2015), this mechanism of action suggested that **147** can
91 influence ER proteostasis through two on-target mechanisms: covalent PDI modification and activation of the
92 UPR-associated transcription factor ATF6. Previous work shows that **147** protected cardiomyocytes both in
93 vitro and in vivo from pathologic insults through an ATF6-dependent mechanism (Blackwood, Azizi et al.,
94 2019), highlighting the potential for **147**-dependent ATF6 activation to promote protective signaling. However,
95 the potential to influence ER proteostasis of secretory proteins through **147**-dependent PDI modification had
96 not been previously demonstrated.

97 Here, we show that compound **147** reduces the secretion of the destabilized, amyloidogenic λ6a LC
98 ALLC from AL patient-derived plasma cells. However, this **147**-dependent reduction in ALLC secretion is
99 refractory to co-treatments with ATF6 inhibitors, demonstrating that this compound reduces ALLC secretion
100 through an ATF6-independent mechanism. Instead, our results indicate that **147** reduces ALLC plasma cell
101 secretion through an on-target mechanism involving metabolic activation and covalent modification of multiple
102 PDIs. Consistent with this, other PDI inhibitors that covalently modify a similar subset of PDIs also reduce
103 ALLC plasma cell secretion through a mechanism analogous to that observed for **147**. These results indicate
104 that pharmacologic targeting of PDIs using ER proteostasis regulators like **147** represents a potential strategy
105 to mitigate the plasma cell secretion of amyloidogenic LCs implicated in AL. Importantly, we further show that
106 **147** is compatible with chemotherapeutics used to ablate AL plasma cells (e.g., bortezomib), indicating that
107 these two approaches could be used in combination to reduce both the LC-associated organ toxicity and
108 underlying plasma cell malignancy observed in AL pathogenesis. Ultimately, our results demonstrate that,
109 apart from promoting ATF6-mediated ER proteostasis remodeling, compound **147** can also correct pathologic
110 imbalances in ER proteostasis through the covalent targeting of PDIs. This highlights the broad potential for
111 this compound to influence ER proteostasis for structurally diverse proteins implicated in many types of protein
112 misfolding disease.
113
114

115 **RESULTS**

116 ***Compound 147 reduces ALLC secretion from AL patient plasma cells***

117 We previously showed that **147** reduces secretion of the amyloidogenic λ6a LC ALLC from AL patient-derived
118 ALMC-2 cells by 50% (Plate et al., 2016). We confirmed this **147**-dependent reduction in ALLC secretion by
119 both immunoblotting and ELISA (**Figure 1A** and **Figure 1 – figure supplement 1A**). However, treatment with
120 **147** did not significantly influence the viability of ALMC-2 cells, indicating that this reduced secretion cannot be
121 attributed to cell death (**Figure 1 – figure supplement 1A**). Compound **147** also did not significantly reduce
122 IgG secretion or cell viability in Multiple Myeloma (MM)-derived KAS-6/1 cells (**Figure 1 – figure supplement**
123 **1B**). This supports previous findings showing that this compound preferentially reduces secretion of
124 destabilized, amyloidogenic LCs (Plate et al., 2016). Amyloidogenic λ LCs are secreted in multiple
125 conformations including monomers, disulfide-bound dimers, and fully assembled IgGs (Kaplan, Ramirez-
126 Alvarado et al., 2009). However, the monomers and dimers are the predominant species associated with toxic
127 LC aggregation and AL amyloid pathology (Andrich, Hegenbart et al., 2017, Brenner et al., 2004, Klimtchuk,
128 Gursky et al., 2010, Ramirez-Alvarado, 2012, Sikkink & Ramirez-Alvarado, 2010). Using non-reducing SDS-
129 PAGE, we showed that **147** reduces secretion of ALLC monomers and dimers from ALMC-2 cells (**Figure**
130 **1B,C**). This demonstrates that this compound decreases extracellular populations of the species most
131 associated with toxic LC aggregation. Using a cycloheximide (CHX) chase assay, we showed that **147** reduces
132 the fraction of ALLC secreted by 30% (**Figure 1D**). However, this reduction in ALLC secretion did not
133 correspond to a significant reduction in total ALLC over the 6 h time course of this experiment, indicating that
134 **147** does not significantly increase ALLC degradation (**Figure 1E**). This result is consistent with previous
135 results, demonstrating that both stress-independent ATF6 activation and treatment with **147** reduces ALLC
136 secretion through a mechanism involving its increased intracellular retention in complexes bound to ER
137 chaperones such as BiP (Plate et al., 2016, Plate et al., 2019).

138

139 ***147 reduces intracellular ALLC in ALMC-2 cells.***

140 Although **147** did not significantly increase ALLC degradation in our CHX experiment, we observed 30-50%
141 reductions in intracellular ALLC in **147**-treated ALMC-2 cells by ELISA and immunoblotting (**Figure 2A** and
142 **Figure 2 – figure supplement 1A**). Co-treatment of **147** with either the proteasome inhibitor MG132 or the

143 lysosome inhibitor chloroquine for 5 h did not influence reductions in intracellular or secreted ALLC (**Figure 2 –**
144 **figure supplement 1A,B**), further indicating that **147** does not increase ALLC degradation over this time
145 course (**Figure 1E**) (Plate et al., 2016). We also did not observe increased recovery of ALLC in cell pellets
146 prepared from **147**-treated ALMC-2 cells, indicating that **147** does not promote intracellular ALLC aggregation
147 (**Figure 2 – figure supplement 1C**). Further, compound **147** did not alter *ALLC* mRNA levels, indicating that
148 reductions in intracellular ALLC cannot be attributed to reduced transcription (**Figure 2 – figure supplement**
149 **1D**). However, we did observe a 20% reduction in both newly-synthesized ALLC and total protein in **147**-
150 treated ALMC-2 cells, as measured by [^{35}S] metabolic labeling (**Figure 2B-D**). This indicates that the reduced
151 intracellular levels of ALLC can in part be attributed to a decrease in translation. Previous work shows that **147**
152 does not reduce translation in other cells including liver-derived HepG2 cells (Plate et al., 2016), indicating that
153 this reduction in protein synthesis is not universally observed in mammalian cells. Co-treatment with ISRIB, a
154 compound that blocks translational attenuation induced by PERK-eIF2α signaling (Sidrauski, Acosta-Alvear et
155 al., 2013, Sidrauski, McGeachy et al., 2015), does not impact the reduction in secreted or intracellular ALLC in
156 **147**-treated ALMC-2 cells (**Figure 2E,F**). This suggests that the reductions in intracellular ALLC are likely
157 independent of PERK-dependent translation attenuation. Collectively, these results show that **147** reduces
158 intracellular ALLC through a mechanism involving reduced translation and that this reduction in synthesis
159 contributes to the reduced ALLC secreted from compound-treated ALMC-2 cells.
160
161 ***147-dependent reductions in ALLC secretion are not dependent on ATF6 activation.***
162 We next defined whether the **147**-dependent reductions in ALLC secretion rely on ATF6 activation. ATF6 is
163 activated through a mechanism involving the reduction of disulfide-linked ATF6 oligomers and increased
164 trafficking of reduced ATF6 monomers to the Golgi (**Figure 3A**) (Koba, Jin et al., 2020, Nadanaka, Okada et
165 al., 2007, Nadanaka, Yoshida et al., 2006, Oka, van Lith et al., 2019). In the Golgi, ATF6 is site-specifically
166 processed by site 1 protease (S1P) and site 2 protease (S2P), releasing the active ATF6 N-terminal bZIP
167 transcription factor domain, which localizes to the nucleus and promotes ATF6 transcriptional activity (Ye,
168 Rawson et al., 2000). Recently, the compound Ceapin-7 (CP7) was shown to stabilize ATF6 oligomers within
169 the ER, preventing ATF6 activation induced by ER stress or ATF6 activating compounds such as **147** (**Figure**
170 **3A**) (Gallagher, Garri et al., 2016, Gallagher & Walter, 2016, Paxman et al., 2018, Torres, Gallagher et al.,

171 2019). We confirmed that co-treatment of ALMC-2 cells with CP7, but not the inactive analog CP5 (**Figure 3 –**
172 **figure supplement 1**), blocked **147**-dependent increases in the ATF6 target gene *BiP* (**Figure 3B**).
173 Interestingly, co-treatment with CP7 did not block **147**-dependent reductions in ALLC secretion from ALMC-2
174 cells (**Figure 3C**). Further, co-treatment with CP7 did not influence **147**-dependent reductions in intracellular
175 ALLC (**Figure 3D**). This suggests that **147** reduces ALLC secretion through a mechanism independent of
176 ATF6. To further probe this prediction, we co-treated ALMC-2 cells with **147** and the S1P inhibitor PF429242
177 (S1Pi), a compound that blocks ATF6 activation through a mechanism distinct from CP7 (**Figure 3A**) (Hay,
178 Abrams et al., 2007, Lebeau, Byun et al., 2018). Co-treatment with S1Pi also did not block **147**-dependent
179 reductions in secreted ALLC (**Figure 3E**). These results further confirm that **147** reduces ALLC secretion from
180 ALMC-2 cells through a mechanism independent of ATF6 activation.
181
182 ***147 reduces ALLC secretion through an on-target mechanism involving metabolic activation and***
183 ***covalent protein modification.***
184 Compound **147** activates ATF6 through a mechanism involving metabolic oxidation to a quinone methide (**147-**
185 **QM**) and subsequent covalent modification of ER-localized proteins including multiple PDIs (**Figure 4A**)
186 (Paxman et al., 2018). This activation mechanism requires the 2-amino-*p*-methyl cresol moiety of the **147** 'A-
187 ring' (**Figure 4A**). To define a structure-activity relationship for **147**-dependent reductions in ALLC secretion,
188 we screened **147** analogs to define their ability to reduce ALLC secretion from ALMC-2 cells (Paxman et al.,
189 2018). Compounds containing alterations to the **147** 2-amino-*p*-methyl cresol 'A-ring' did not reduce ALLC
190 secretion, indicating that this ring is required for compound activity in this assay (**Figure 4B**). Similarly, analogs
191 that include alterations to the **147** 'linker' did not substantially reduce ALLC secretion (**Figure 4A** & **Figure 4 –**
192 **figure supplement 1A**). However, analogs containing alterations to the **147** 'B-ring' showed varying levels of
193 efficacy in reducing ALLC secretion from ALMC-2 cells (**Figure 4A** & **Figure 4 – figure supplement 1B**). This
194 structure-activity relationship is identical to that previously established for **147**-dependent ATF6 activation
195 (Paxman et al., 2018). Consistent with this, we observe an inverse correlation between analog-dependent
196 activation of an ATF6 reporter in HEK293 cells (Paxman et al., 2018) and reductions in ALLC secretion from
197 ALMC-2 cells (**Figure 4C**). This suggests that **147** reduces ALLC secretion from ALMC-2 cells through the
198 same mechanism required for ATF6 activation (**Figure 4A**).

199 The activation of ATF6 by **147** can be inhibited by co-administration of resveratrol or β-mercaptoethanol
200 (BME), which block different steps of the compound activation mechanism (**Figure 4A**) (Paxman et al., 2018).
201 Thus, we sought to define how treatment with resveratrol or BME influences **147**-dependent reduction in ALLC
202 secretion from ALMC-2 cells. Interestingly, co-treatment with BME or resveratrol blocked **147**-dependent
203 reductions in ALLC secretion (**Figure 4D,E**). Neither BME nor resveratrol impacted ALMC-2 cell viability in the
204 absence or presence of **147** (**Figure 4 – figure supplement 1C,D**). Similar results were observed for ALMC-2
205 cells treated with other active analogs of **147** (**Figure 4 – figure supplement 1E**). Importantly, co-treatment
206 with resveratrol or BME also blocked the **147**-dependent reductions in intracellular ALLC measured by ELISA
207 (**Figure 4 – figure supplement 1F**). Resveratrol also inhibited the translation attenuation in **147**-treated
208 ALMC-2 cells measured by [^{35}S] metabolic labeling (**Figure 4 – figure supplement 1G**). These results further
209 demonstrate that **147** reduces ALLC secretion from ALMC-2 cells through the same mechanism required for
210 ATF6 activation, involving both compound metabolic activation and covalent protein modification (**Figure 4A**).
211

212 ***Compound 147 alters interactions between ALLC and ER PDIs.***

213 The above results indicate that **147**-dependent reduction in ALLC secretion from ALMC-2 cells requires
214 covalent modification of proteins. We previously identified proteins modified by **147** using an alkyne-modified
215 analog (**147-alkyne; Figure 5 – figure supplement 1A,B**) (Paxman et al., 2018). **147-alkyne** reduces ALLC
216 secretion from ALMC-2 cells to levels identical to that observed for **147**, indicating that these compounds have
217 similar activities (**Figure 5 – figure supplement 1C**). Three predominant proteins modified by **147-alkyne** in
218 ALMC-2 cells are PDIA1, PDIA4, and PDIA6 (**Figure 5 – figure supplement 1B)** (Paxman et al., 2018).
219 Importantly, addition of excess parent compound **147** competes the labeling of these PDIs by **147-alkyne**,
220 confirming on-target activity (**Figure 5 – figure supplement 1D**) (Paxman et al., 2018). However, we did not
221 observe significant labeling of ALLC in ALMC-2 cells (**Figure 5 – figure supplement 1B,D**) (Paxman et al.,
222 2018). This indicates that **147** influences ALLC secretion from ALMC-2 cells by targeting the activity of PDIs,
223 rather than direct targeting of ALLC. Consistent with this, pharmacologic inhibition of PDIA1 was previously
224 shown to reduce ALLC secretion from HEK293T cells (Cole, Grandjean et al., 2018) and ATF6-dependent
225 reductions in ALLC secretion from HEK293 cells correlate to increased interactions with PDIA4 (Plate et al.,
226 2019). Thus, we sought to define how **147** influences interactions between ALLC and these two PDIs.

227 Interestingly, **147** reduces ALLC interactions with PDIA1 by 25%, while increasing interactions with PDIA4 65%
228 (**Figure 5A,B** and **Figure 5 – figure supplement 1E**). Both of these changes correspond with the alterations
229 in ALLC interactions previously suggested to decrease ALLC secretion (Cole et al., 2018, Plate et al., 2019).
230 This suggests that **147** could reduce ALLC secretion through an ATF6-independent mechanism involving
231 covalent modification of these PDIs.

232 RNAi-depletion of PDIs (including *PDIA1* and *PDIA4*) can induce ER stress and subsequent UPR
233 activation (Paxman et al., 2018), challenging our ability to define the specific contributions of individual PDIs in
234 the **147**-dependent reduction in ALLC secretion from ALMC-2 cells. Thus, in order to define how
235 pharmacologic targeting of PDIs influence ALLC secretion, we used structurally distinct PDI inhibitors that
236 covalently modify a similar subset of PDIs to **147**. Recently, the compound RB-11-ca and its more selective
237 analog KSC-34 were identified to covalently modify PDIA1 (**Figure 5 – figure supplement 1F**) (Banerjee,
238 Pace et al., 2013, Cole et al., 2018). These compounds contain an alkyne moiety that allows us to rapidly
239 define their modification of different PDIs using an approach identical to that employed for **147-alkyne** (**Figure**
240 **5 – figure supplement 1B**). While RB-11-ca and KSC-34 show increased background labeling relative to **147-**
241 **alkyne**, both of these compounds label bands that correspond to the three predominant PDIs modified by **147**,
242 PDIA1, PDIA4, and PDIA6, albeit to different extents (**Figure 5C,D**). RB-11-ca and KSC-34 modified PDIA1 to
243 higher levels than **147-alkyne**, consistent with their selectivity for this PDI (Banerjee et al., 2013, Cole et al.,
244 2018). Alternatively, RB-11-ca labeled PDIA4 and PDIA6 to levels 70-85% that observed for **147-alkyne**,
245 whereas KSC-34 showed lower levels of labeling for these PDIs. This is consistent with the increased
246 selectivity of KSC-34 for PDIA1 relative to RB-11-ca (Cole et al., 2018). Collectively, these results show that
247 KSC-34 and, more specifically, RB-11-ca covalently modify similar PDIs to those modified by **147-alkyne**,
248 providing a complementary approach to define how covalent targeting of PDIs impact ALLC secretion from
249 ALMC-2 cells.
250

251 ***Pharmacologic PDI inhibition reduces ALLC secretion from ALMC-2 cells.***

252 Interestingly, both RB-11-ca and KSC-34 reduced ALLC secretion from ALMC-2 cells, as measured by ELISA
253 (**Figure 6A**). RB-11-ca reduced ALLC secretion by 35%, whereas KSC-34 reduced ALLC secretion by 25%.
254 Importantly, this reduction in secretion did not correspond to reductions in ALMC-2 cell viability (**Figure 6 –**

255 **figure supplement 1A**). Similar reductions in ALLC secretion were observed for RB-11-ca by immunoblotting
256 (**Figure 6 – figure supplement 1B**). As with **147**, RB-11-ca reduced secretion of ALLC dimers and monomers,
257 demonstrating that this PDI inhibitor reduces secretion of ALLC in the conformations most commonly linked to
258 AL pathogenesis (**Figure 6B,C**). This reduction in ALLC secretion also corresponds with reductions in
259 intracellular ALLC measured with immunoblotting (**Figure 6D**) and reductions in protein translation measured
260 by [^{35}S] labeling (**Figure 6 – figure supplement 1C**), mimicking the results observed with **147**. Furthermore,
261 RB-11-ca reduced ALLC interactions with PDIA1 and increased interactions with PDIA4 (**Figure 6E,F**).
262 However, neither compound significantly influenced ALLC interactions with PDIA6. Again, these changes are
263 analogous to those observed with **147** (**Figure 5A,B**). However, the reduction in ALLC interactions with PDIA1
264 was greater than that observed for **147**, likely reflecting the increased labeling of PDIA1 by RB-11-ca (**Figure**
265 **5C,D**). These results indicate that pharmacologic targeting PDIs with other PDI inhibitors reduces ALLC
266 secretion from ALMC-2 cells through a mechanism analogous to that observed for **147**. This supports a model
267 whereby **147** reduces ALLC secretion through an on-target ATF6-independent mechanism involving covalent
268 modification of multiple PDIs.
269
270 ***147-dependent reductions in ALLC secretion are compatible with bortezomib-induced ablation of AL***
271 ***plasma cell.***
272 In order to improve the treatment of AL patients in the clinic, any treatment strategy designed to ameliorate AL
273 amyloid pathology must be compatible with standard chemotherapeutics such as the proteasome inhibitor
274 bortezomib used to target the underlying plasma cell malignancy (Gupta, Brauneis et al., 2019, Kastritis et al.,
275 2019, Manwani et al., 2018, Salinaro et al., 2017). Bortezomib induces toxicity in plasma cells through a
276 mechanism involving inhibition of ER-associated degradation and increased ER stress (Nikesitch, Lee et al.,
277 2018, Obeng, Carlson et al., 2006, Ri, 2016). Compound **147** promotes adaptive ER proteostasis remodeling
278 in ALMC-2 plasma cells through both covalent PDI modification and ATF6 activation, suggesting that treatment
279 with this compound could reduce bortezomib-induced toxicity in AL-associated plasma cells. To test this, we
280 evaluated the viability of ALMC-2 cells co-treated with bortezomib and **147**. Bortezomib induces toxicity in
281 ALMC-2 cells with an EC_{50} of 45 nM (**Figure 7A,B**). While **147** treatment alone showed a modest ~15%
282 reduction in ALMC-2 viability (as reported previously (Plate et al., 2016)), this compound did not significantly

283 influence bortezomib-induced toxicity in these cells (**Figure 7A,B**). Furthermore, **147** did not increase or
284 decrease activation of the pro-apoptotic caspases 3/7 in ALMC-2 cells co-treated with subtoxic or toxic doses
285 of bortezomib, respectively (**Figure 7C**). These results indicate that **147** does not interfere with bortezomib-
286 induced plasma cell cytotoxicity and that these two compounds have the potential to be used in combination to
287 mitigate both the amyloid pathology and plasma cell malignancy associated with AL pathogenesis.
288

289 **DISCUSSION**

290 Compound **147** was established as a tool to pharmacologically induce preferential activation of the ATF6 UPR
291 signaling pathway (Paxman et al., 2018, Plate et al., 2016). In this role, **147** has proven useful for probing the
292 therapeutic potential for pharmacologic ATF6 activation in human disease. For example, **147** was used to
293 demonstrate that pharmacologic ATF6 activation protects against ischemia and reperfusion (I/R) injury in both
294 primary cardiomyocytes and in vivo mouse models of myocardial infarction (Blackwood et al., 2019). Genetic
295 depletion or cardiac-specific knockout of *Atf6* blocked **147**-dependent protection in these models,
296 demonstrating that this **147** protection requires ATF6 signaling. Similarly, **147**-dependent ATF6 activation was
297 shown to alter stem cell differentiation, revealing new roles for ATF6 signaling in development (Kroeger,
298 Grimsey et al., 2018). These results highlight the potential for **147**-dependent ATF6 activation to influence
299 physiologic and pathologic processes in diverse biologic contexts.

300 Here, we show that **147** reduces the plasma cell secretion of destabilized, amyloidogenic ALLC through
301 an on-target, ATF6-*independent* mechanism that involves covalent modification of multiple PDIs. PDIs
302 primarily function in ER proteostasis by regulating the formation of disulfide bonds within secretory proteins,
303 although many PDIs have chaperoning activity that is independent of their redox function (Appenzeller-Herzog
304 & Ellgaard, 2008, Wang et al., 2015). Interestingly, **147** alters the interactions between ALLC and multiple PDIs
305 (e.g., PDIA1 and PDIA4) in ways that are consistent with reduced LC secretion. PDIA1 facilitates LC folding in
306 the early secretory pathway (Borth, Mattanovich et al., 2005, Lilie, McLaughlin et al., 1994). This suggests that
307 reductions in PDIA1 activity should reduce plasma cell secretion of amyloidogenic LCs. Consistent with this,
308 PDIA1 inhibitors decrease ALLC secretion from HEK293 cells (Cole et al., 2018). This indicates that the
309 reduced interaction between ALLC and PDIA1 afforded by **147** contributes to the reduced secretion of ALLC
310 from AL patient plasma cells. Conversely, ALLC increased interactions with PDIA4 in **147**-treated ALMC-2
311 cells. This is consistent with the increased interactions between ALLC and PDIA4 observed in HEK293 cells
312 following stress-independent ATF6 activation – a treatment where ALLC secretion is reduced through its
313 increased ER retention in chaperone bound complexes (Plate et al., 2019). Interestingly, PDIA4 has been
314 implicated in the retention of misfolded proteins within the ER (Forster, Sivick et al., 2006, Sorensen, Ranheim
315 et al., 2006), suggesting that the increased interaction between ALLC and PDIA4 in **147**-treated ALMC-2 cells
316 likely contributes to the **147**-dependent ER retention of ALLC in ALMC-2 cells. Collectively, these results

317 indicate that **147**-dependent alterations in the activity of multiple PDIs contribute to the reduced secretion of
318 ALLC from AL patient derived plasma cells.

319 We further defined the importance of PDIs in the plasma cell secretion of ALLC by showing that
320 structurally distinct PDI inhibitors similarly reduce ALLC secretion from ALMC-2 plasma cells. Interestingly, RB-
321 11-ca reduces ALLC secretion through a mechanism analogous to that observed for **147** involving both
322 increased ALLC interactions with PDIA4 and reduced interactions with PDIA1. Furthermore, RB-11-ca reduces
323 intracellular ALLC and induces translational attenuation in ALMC-2 cells, again mirroring results observed for
324 **147**. While the mechanistic basis of this translational attenuation remains to be defined, our results showing
325 that two structurally distinct PDI modifying compounds both reduce protein translation in ALMC-2 cells
326 indicates that this reduced synthesis likely results from PDI modification. Collectively, these results further
327 support a model whereby pharmacologic targeting of multiple PDIs is the primary mechanism responsible for
328 the **147**-dependent reduction in ALLC secretion from ALMC-2 plasma cells.

329 These results indicate that PDI inhibitors such as **147** or RB-11-ca offer unique opportunities to reduce
330 the secretion and toxic aggregation of amyloidogenic LCs implicated in AL pathogenesis. However, **147** has
331 advantages over other available PDI inhibitors that make it particularly suitable for further translational
332 development. For example, **147** is metabolically activated to its reactive form on the ER membrane (Paxman et
333 al., 2018). This localized activation allows **147** to preferentially modify ER proteins, including many PDIs,
334 minimizing the off-target activity of this compound. This benefit is evident by the reduced background labeling
335 observed when comparing proteins modified by **147** and RB-11-ca. Furthermore, **147** shows reduced labeling
336 of PDIA1 relative to RB-11-ca. Since PDIA1 is important for the folding and trafficking of numerous secretory
337 proteins including insulin (Jang, Pottekat et al., 2019), the reduced targeting of PDIA1 by **147** will minimize
338 potential consequences associated with inhibiting PDIA1 in vivo. Consistent with this, **147** administration has
339 not been associated with any in vivo toxicity to date (Blackwood et al., 2019). Thus, while many different PDI
340 inhibitors have been developed, these unique properties of **147** make it an attractive compound for
341 pharmacologically targeting PDIs to influence ER proteostasis in diseases like AL.

342 Importantly, we show that **147** reduces secretion of ALLC in dimeric and monomeric conformations –
343 the two conformations most associated with LC proteotoxicity in AL pathogenesis (Andrich et al., 2017,
344 Brenner et al., 2004, Klimtchuk et al., 2010, Ramirez-Alvarado, 2012, Sikkink & Ramirez-Alvarado, 2010). This

345 is consistent with previous results showing that **147** reduces the extracellular aggregation of ALLC secreted
346 from ALMC-2 plasma cells (Plate et al., 2016). Moreover, we demonstrate that **147** does not influence the
347 bortezomib-induced toxicity in ALMC-2 cells, indicating that these two compounds have potential to be used in
348 combination to treat AL in the patients. In this combination approach, **147** would be administered to reduce LC-
349 associated proteotoxicity on distal tissues such as the heart while chemotherapeutics such as bortezomib
350 would be administered to ablate the underlying cancerous plasma cell population. This combined strategy
351 provides the opportunity to both mitigate the LC-associated proteotoxicity and provide chemotherapeutic
352 access to the underlying diseased plasma cells in the 30% of patients suffering from severe LC-associated
353 proteotoxicity. Thus, our results further support the potential application of compounds like **147** for the
354 treatment of AL and reveal new mechanistic insights into compound-dependent reductions in ALLC secretion
355 that will enable the development of next generation compounds with improved translational potential for this
356 disease.
357
358
359
360

361 **MATERIALS AND METHODS**

362 ***Chemicals***

363 Compound **147**, **147-alkyne**, and all **147** analogs were synthesized in house and are described in (Paxman et
364 al., 2018). RB-11-ca and KSC-34 were both kind gifts from Eranthie Weerapana at Boston College (Banerjee
365 et al., 2013, Cole et al., 2018). Ceapin-7 (CP7) and Ceapin-5 (CP5) were kind gifts from Peter Walter at UCSF
366 (Gallagher et al., 2016, Gallagher & Walter, 2016). Cycloheximide (Fisher), resveratrol (SelleckChem), ISRIB
367 (Sigma), MG132 (Selleckchem), chloroquine (Sigma), PF429242 (S1Pi; Tocris), β-mercaptoethanol (BME;
368 Thermo Fisher), and bortezomib (MilliporeSigma) were all purchased commercially.

369

370 ***Antibodies***

371 All antibodies were commercially purchased. Antibodies were used for immunoblotting at the indicated dilution:
372 mouse human lambda light chain antibody (Novus Biological, NBP2-29462, 1:250); rabbit PDIA1 (PDI)
373 antibody (GeneTex, GTX101468, 1:1000), rabbit PDIA4 (ERP72) antibody (ProteinTech, 14712-1-AP, 1:1000)
374 and mouse PDIA6 antibody (ProteinTech 66669-1-Ig, 1:1000).

375

376 ***Cell Lines and Culture Conditions***

377 ALMC-2 and KAS-6/1 plasma cells were a kind gift from Diane Jelinak (Arendt, Ramirez-Alvarado et al., 2008).
378 We cultured these two plasma cell lines in Iscove's Modified Dulbecco's Media (IMDM) GlutMAX (Life
379 Technologies) supplemented with penicillin/streptomycin, 5% fetal bovine serum, and 2 ng/mL interleukin-6 (IL-
380 6), following published protocols (Arendt et al., 2008, Plate et al., 2016). Cells were cultured at 37°C with 5%
381 CO_2.

382

383 ***ELISA***

384 The ELISA for ALLC and fully-assembled IgGs in conditioned media prepared on ALMC-2 or KAS-6/1 cells
385 was performed using an identical approach to that reported in (Plate et al., 2016). Briefly, ALMC-2 or KAS-6/1
386 plasma cells were plated 100,000 cells/well in 150 µL of media in 96-well MultiScreen$_{HTS}$ filtration plates
387 (EMD Millipore). Five replicates were treated with DMSO or compounds at the indicated concentrations and
388 incubated for 18 hr. Media was removed by filtration using a QIAvac 96 vacuum manifold (Qiagen) and wells

389 were washed two times with 150 µL media. Wells were then incubated with 150 µL of fresh media for 2 hr and
390 the conditioned media was harvested into a 96-well plate using the vacuum manifold. Whole lysates were
391 obtained by adding RIPA buffer to the cells in the filtration plates. Free LC and IgG concentrations were
392 determined by ELISA in 96-well plates (Immulon 4HBX, Thermo Fisher). Wells were coated overnight at 37 ºC
393 with sheep polyclonal free λ LC antibody (Bethyl Laboratories, A80-127A) at a 1:500 dilution or human IgG-
394 heavy and light chain antibody (Bethyl Laboratories, A80-118A) at a 1:2000 dilution in 50 mM sodium
395 carbonate (pH 9.6). In between all incubation steps, the plates were rinsed extensively with Tris-buffered saline
396 containing 0.05% Tween-20 (TBST). Plates were blocked with 5% non-fat dry milk in TBST for 1 hr at 37ºC.
397 Media analytes were diluted between 5 – 200 fold in 5% non-fat dry milk in TBST and 100 µL of each sample
398 was added to individual wells. Light chain or IgG standards ranging from 3 – 300 ng/mL were prepared from
399 purified human Bence Jones λ light chain or human reference serum (Bethyl Laboratories, P80-127 and RS10-
400 110). Plates were incubated at 37 ºC for 1.5 hr while shaking. Finally, HRP-conjugated goat anti-human λ light
401 chain antibody (Bethyl Laboratories, A80-116P) was added at a 1:5,000 dilution or HRP-conjugate IgG-Fc
402 fragment cross-adsorbed antibody (Bethyl Laboratories, A80-304P, 1:30,000 dilution) was added in 5% non-fat
403 dry milk in TBST, followed by a 1.5 hr incubation of the plates at 37 ºC. The detection was carried out with 2,2'-
404 azinobis (3-ethylbenzothiazoline-6-sulfonic acid) (ABTS, 0.18 mg/mL) and 0.03% hydrogen peroxide in
405 100 mM sodium citrate pH 4.0. Detection solution (100 µL) was added to each well and the plates were
406 incubated at room temperature. The absorbance was recorded at 405 nm and the values for the LC standards
407 were fitted to a 4-parameter logistic function. Light chain or IgG concentrations were averaged from at least 3
408 independent replicates under each treatment and then normalized to vehicle conditions.
409

410 ***Immunoblotting for ALLC***

411 Conditioned media was collected from ALMC-2 cells as previously described (Plate et al., 2016). Media was
412 denatured with Laemmli buffer + 100 mM DTT and boiled for 5 min prior to being separated by SDS-PAGE.
413 Conditioned media for non-reducing gels were prepared as above in the absence of DTT. Cell lysates were
414 prepared as previously described (Plate et al., 2016) in RIPA buffer with fresh protease inhibitor cocktail
415 (Roche). Total protein concentration in cellular lysates was normalized using the Bio-Rad protein assay.
416 Lysates were then denatured with Laemmli buffer + 100 mM DTT and boiled for 5 min before being separated

417 by SDS-PAGE. Proteins were then transferred onto nitrocellulose membranes (Bio-Rad) for immunoblotting
418 and blocked with 5% milk in Tris-buffered saline, 0.5 % Tween-20 (TBST). Membranes were then incubated
419 overnight at 4°C with primary antibodies. Membranes were washed in TBST, incubated with IR-Dye
420 conjugated secondary antibodies and analyzed using Odyssey Infrared Imaging System (LI-COR Biosciences).
421 Quantification was carried out with LI-COR Image Studio software.

422 To measure intracellular ALLC aggregation, ALMC-2 cells were lysed in RIPA buffer as described
423 above. Following centrifugation at 20,000 g for 10 min, we collected the soluble supernatant fraction (SN). We
424 then resuspended the pellet in RIPA + 2% SDS and DTT and sonicated to release aggregate protein. SN and
425 resolubilized pellets were then separated by SDS-PAGE and probed by immunoblotting as above.

426

427 ***ALLC Immunopurification.***

428 ALLC was co-purified with ER proteostasis factors using an identical strategy to that previously reported (Plate
429 et al., 2016). Briefly, ALMC-2 cells were treated for 30 min a room temperature with PBS containing the
430 reversible crosslinker dithiobis (succinimidiyl propionate) (DSP, Thermo Scientific, 500 μM). This crosslinking
431 reaction was quenched by addition of 100 mM Tris pH 7.5 for 15 min. Lysates were then prepared in RIPA
432 buffer, as above. Total protein concentration in cellular lysates was normalized using Bio-Rad protein assay.
433 Cell lysates were then subjected to preclearing with Sepharose 4B beads (Sigma) at 4 °C for 1 h with agitation.
434 Lysates were then incubated overnight at 4 °C with Protein A beads coupled to λ LC antibody, as described
435 below. After four washes in RIPA buffer, crosslinks were cleaved and proteins were eluted by boiling in
436 Laemmli buffer with 100 mM DTT. Eluates were then separated by SDS-PAGE and immunoblotted as
437 described above. Quantifications of proteins co-purified with ALLC were normalized to the recovered ALLC, as
438 described previously (Plate et al., 2019).

439 For immunopurification, protein A Sepharose 4B beads (101041, Thermo Fisher) were coupled to
440 human lambda light chain antibody (A80-112A, Bethyl laboratories) (Plate et al., 2016). Briefly, beads were
441 washed twice with RIPA buffer (50 mM Tris, pH 7.5, 150 mM NaCl, 0.1 % SDS, 1% Triton X-100, 0.5%
442 deoxycholate) and resuspended in 1 mL of PBS. Beads were then incubated with primary rabbit human
443 lambda light chain antibody (40 uL of antibody for 70-90- μL of beads) and rocked for 1 hour at room
444 temperature. Beads were washed 3 times with 0.2M borate buffer pH = 9. The antibody was crosslinked to the

445 beads by incubating with 20 mM of the crosslinker dimethyl pimelimidate (DMP, Thermo Scientific, 20 μM) for
446 30 min at room temperature. The crosslinking reaction was stopped by incubation with 0.2 M ethanolamine pH
447 8 for 2 h at room temperature. Beads were then washed with Glycine buffer (0.1M, pH=3) to remove
448 uncrosslinked antibody, followed by two washes with PBS. Finally, beads were resuspended in storage buffer
449 (PBS, Azide (0.01%)) and stored at 4ºC.
450
451 ***Quantitative RT-PCR***
452 The mRNA levels of target genes were measured using quantitative RT-PCR on an ABI 7900HT Fast Real
453 Time PCR machine using the same primers and identical approach to that published in (Plate et al., 2016).
454
455 ***Cell Viability and Apoptosis Assays.***
456 ALMC-2 cells were plated at 33,000 cells/well in a translucent, flat-bottomed 96 well plate, and treated for 18 hr
457 with vehicle, 147 (10 μM) or bortezomib (at the indicated doses). After incubation, cell metabolic activity or
458 caspase 3/7 activity was measured using the CellTiter-Glo assay (Promega) and Caspase-Glo 3/7 assay
459 (Promega), respectively, according to the manufacturer's instructions. Briefly, the plates containing cells were
460 removed from the incubator and allowed to equilibrate to room temperature for 30 min. CellTiter-Glo or
461 Caspase-Glo reagent was added to each well at a 1:1 v/v ratio and incubated for 2 min on an orbital shaker to
462 induce cell lysis. The plate was then incubated at room temperature for 10 min to stabilize the luminescent
463 signal and read on a Tecan F200 Pro microplate reader.
464
465 ***[^{35}S] Metabolic Labeling***
466 For metabolic labeling experiments, ALMC-2 cells were plated at a density of $1x10^6$ cells/well on a 6 well plate.
467 Cells were then treated with **147** (10 μM), RB-11-ca (30 μM), and/or resveratrol (10 μM), as indicated. Cells
468 were transferred to microfuge tubes, washed with PBS, and metabolically labeled in DMEM-Cys/-Met (Corning)
469 supplemented with glutamine, penicillin/streptomycin, dialyzed fetal bovine serum, and EasyTag EXPRESS
470 [^{35}S] Protein Labeling Mix (Perkin Elmer) for 30 min in a tissue culture incubator. Cells were washed twice with
471 PBS and lysates were harvested using RIPA buffer (50 mM Tris, pH 7.5, 150 mM NaCl, 0.1 % SDS, 1% Triton
472 X-100, 0.5% deoxycholate) and protease inhibitor cocktail (Roche). ALLC was immunopurified using human

473 lambda LC coupled to Protein A Sepharose beads as described above. Lysates were incubated with the beads
474 overnight at 4 degrees. Beads were washed 5 times with RIPA buffer. ALLC was then isolated by boiling in
475 Laemmli buffer + 100 mM DTT and separated on SDS-PAGE. For whole cell lysates, cells were lysed in RIPA
476 buffer. Laemmli buffer + 100 mM DTT was then added to the lysates and separated by SDS-PAGE. All gels
477 were dried, exposed to phosphorimager plates (GE Healthcare), and imaged with a Typhoon imager. Band
478 intensities were quantified by densitometry in ImageQuant.
479

480 ***Profiling of Targets for 147 and PDI Inhibitors***

481 Proteins labeled by treatment with **147-alkyne**, RB-11-ca, or KSC34 in were performed as previously
482 described (Paxman et al., 2018). Briefly, ALMC-2 cells in 6-well plates were treated for 18 h with **147-alkyne**
483 (10uM), RB-11-ca (30 μM) or KSC-34 (30 μM). Lysates were then prepared in RIPA buffer as described above.
484 Protein concentrations were then quantified by Bradford. Lysates containing 50 μg of protein were then
485 incubated for 2 h with shaking at 37°C with 100 μM TAMRA azide (Click Chemistry Tools Scottsdale, Az), 800
486 μM copper(II) sulfate, 1.6 mM BTTAA ligand (2-(4-((bis((1-tert-butyl-1H-1,2,3-triazol-4-
487 yl)methyl)amino)methyl)−1 H-1,2,3-triazol-1-yl)acetic acid) (Click Chemistry Tools Scottsdale, Az), and 5 mM
488 sodium ascorbate. Samples were then boiled with Laemmli Buffer and 100mM DTT and separated by SDS-
489 PAGE. TAMRA-labeled proteins were then imaged using a Bio-Rad ChemiDoc using the rhodamine channel.
490

491 ***Statistical Methods***

492 Replicates for each experiment comprise cells in separate wells/dishes that were treated independently. The
493 number of replicates and independent experiments for each figure panel are clearly stated in the figure
494 legends. Unless otherwise noted, all p-values were calculated by performing a two-tailed paired or two-tailed
495 unpaired t-test.
496
497
498
499

ACKNOWLEDGEMENTS. We thank Evan Powers and Jessica Rosarda for critical reading of the manuscript and Kelly Chen for experimental support. We thank Diane Jelinak (Mayo) for providing the ALMC-2 and KAS-6/1 cell lines, Eranthie Weerapana (Boston College) for RB-11-ca and KSC-34, and Peter Walter (UCSF) for providing CP7 and CP5. This work was funded by the NIH (DK107604 to RLW), a Leukemia & Lymphoma Society Postdoctoral Fellowship (to BR), and an American Heart Association Predoctoral Fellowship (to ICR).

AUTHOR CONTRIBUTIONS.

BR, JSM, ICR, and RLW conceptualized the experiments and performed formal analysis of the primary data. BR, JSM performed the experiments. RJP and JWK provided resources and developed methodology used in this manuscript. BR and RLW wrote the manuscript and all authors were involved in the review and editing. RLW was responsible for supervision, administration, and funding acquisition for the work described in this manuscript.

COMPETING INTEREST STATEMENT.

Jeffrey W. Kelly is a co-founder of Proteostasis Therapeutics Inc. A patent (WO20171174301A1) describing the use of ER proteostasis regulators including **147** to treat protein misfolding diseases includes Ryan J. Paxman, Jeffery W. Kelly, and R. Luke Wiseman as inventors. No other competing interests are declared.

520 **REFERENCES**

521 Andrich K, Hegenbart U, Kimmich C, Kedia N, Bergen HR, 3rd, Schonland S, Wanker E, Bieschke J (2017)
522 Aggregation of Full-length Immunoglobulin Light Chains from Systemic Light Chain Amyloidosis (AL) Patients
523 Is Remodeled by Epigallocatechin-3-gallate. *J Biol Chem* 292: 2328-2344
524 Appenzeller-Herzog C, Ellgaard L (2008) The human PDI family: versatility packed into a single fold. *Biochim*
525 *Biophys Acta* 1783: 535-48
526 Arendt BK, Ramirez-Alvarado M, Sikkink LA, Keats JJ, Ahmann GJ, Dispenzieri A, Fonseca R, Ketterling RP,
527 Knudson RA, Mulvihill EM, Tschumper RC, Wu X, Zeldenrust SR, Jelinek DF (2008) Biologic and genetic
528 characterization of the novel amyloidogenic lambda light chain-secreting human cell lines, ALMC-1 and ALMC-
529 2. *Blood* 112: 1931-41
530 Badar T, D'Souza A, Hari P (2018) Recent advances in understanding and treating immunoglobulin light chain
531 amyloidosis. *F1000Res* 7
532 Banerjee R, Pace NJ, Brown DR, Weerapana E (2013) 1,3,5-Triazine as a modular scaffold for covalent
533 inhibitors with streamlined target identification. *J Am Chem Soc* 135: 2497-500
534 Blackwood EA, Azizi K, Thuerauf DJ, Paxman RJ, Plate L, Kelly JW, Wiseman RL, Glembotski CC (2019)
535 Pharmacologic ATF6 activation confers global protection in widespread disease models by reprograming
536 cellular proteostasis. *Nat Commun* 10: 187
537 Blancas-Mejia LM, Misra P, Dick CJ, Cooper SA, Redhage KR, Bergman MR, Jordan TL, Maar K, Ramirez-
538 Alvarado M (2018) Immunoglobulin light chain amyloid aggregation. *Chem Commun (Camb)* 54: 10664-10674
539 Blancas-Mejia LM, Ramirez-Alvarado M (2013) Systemic amyloidoses. *Annu Rev Biochem* 82: 745-74
540 Borth N, Mattanovich D, Kunert R, Katinger H (2005) Effect of increased expression of protein disulfide
541 isomerase and heavy chain binding protein on antibody secretion in a recombinant CHO cell line. *Biotechnol*
542 *Prog* 21: 106-11
543 Braakman I, Bulleid NJ (2011) Protein folding and modification in the mammalian endoplasmic reticulum. *Annu*
544 *Rev Biochem* 80: 71-99
545 Brenner DA, Jain M, Pimentel DR, Wang B, Connors LH, Skinner M, Apstein CS, Liao R (2004) Human
546 amyloidogenic light chains directly impair cardiomyocyte function through an increase in cellular oxidant stress.
547 *Circ Res* 94: 1008-10
548 Cohen AD, Comenzo RL (2010) Systemic light-chain amyloidosis: advances in diagnosis, prognosis, and
549 therapy. *Hematology Am Soc Hematol Educ Program* 2010: 287-94
550 Cole KS, Grandjean JMD, Chen K, Witt CH, O'Day J, Shoulders MD, Wiseman RL, Weerapana E (2018)
551 Characterization of an A-Site Selective Protein Disulfide Isomerase A1 Inhibitor. *Biochemistry* 57: 2035-2043
552 Cooley CB, Ryno LM, Plate L, Morgan GJ, Hulleman JD, Kelly JW, Wiseman RL (2014) Unfolded protein
553 response activation reduces secretion and extracellular aggregation of amyloidogenic immunoglobulin light
554 chain. *Proc Natl Acad Sci U S A* 111: 13046-51
555 Dember LM, Sanchorawala V, Seldin DC, Wright DG, LaValley M, Berk JL, Falk RH, Skinner M (2001) Effect
556 of dose-intensive intravenous melphalan and autologous blood stem-cell transplantation on al amyloidosis-
557 associated renal disease. *Ann Intern Med* 134: 746-53
558 Diomede L, Romeo M, Rognoni P, Beeg M, Foray C, Ghibaudi E, Palladini G, Cherny RA, Verga L, Capello
559 GL, Perfetti V, Fiordaliso F, Merlini G, Salmona M (2017) Cardiac Light Chain Amyloidosis: The Role of Metal
560 Ions in Oxidative Stress and Mitochondrial Damage. *Antioxid Redox Signal* 27: 567-582
561 Eisele YS, Monteiro C, Fearns C, Encalada SE, Wiseman RL, Powers ET, Kelly JW (2015) Targeting protein
562 aggregation for the treatment of degenerative diseases. *Nat Rev Drug Discov* 14: 759-80
563 Forster ML, Sivick K, Park YN, Arvan P, Lencer WI, Tsai B (2006) Protein disulfide isomerase-like proteins play
564 opposing roles during retrotranslocation. *J Cell Biol* 173: 853-9
565 Gallagher CM, Garri C, Cain EL, Ang KK, Wilson CG, Chen S, Hearn BR, Jaishankar P, Aranda-Diaz A, Arkin
566 MR, Renslo AR, Walter P (2016) Ceapins are a new class of unfolded protein response inhibitors, selectively
567 targeting the ATF6alpha branch. *Elife* 5
568 Gallagher CM, Walter P (2016) Ceapins inhibit ATF6alpha signaling by selectively preventing transport of
569 ATF6alpha to the Golgi apparatus during ER stress. *Elife* 5
570 Gertz MA (2018) Immunoglobulin light chain amyloidosis diagnosis and treatment algorithm 2018. *Blood*
571 *Cancer J* 8: 44

572 Guan J, Mishra S, Qiu Y, Shi J, Trudeau K, Las G, Liesa M, Shirihai OS, Connors LH, Seldin DC, Falk RH,
573 MacRae CA, Liao R (2015) Lysosomal dysfunction and impaired autophagy underlie the pathogenesis of
574 amyloidogenic light chain-mediated cardiotoxicity. *EMBO Mol Med* 7: 688
575 Guan J, Mishra S, Shi J, Plovie E, Qiu Y, Cao X, Gianni D, Jiang B, Del Monte F, Connors LH, Seldin DC,
576 Lavatelli F, Rognoni P, Palladini G, Merlini G, Falk RH, Semigran MJ, Dec GW, Jr., Macrae CA, Liao R (2013)
577 Stanniocalcin1 is a key mediator of amyloidogenic light chain induced cardiotoxicity. *Basic Res Cardiol* 108:
578 378
579 Gupta VK, Brauneis D, Shelton AC, Quillen K, Sarosiek S, Sloan JM, Sanchorawala V (2019) Induction
580 Therapy with Bortezomib and Dexamethasone and Conditioning with High-Dose Melphalan and Bortezomib
581 Followed by Autologous Stem Cell Transplantation for Immunoglobulin Light Chain Amyloidosis: Long-Term
582 Follow-Up Analysis. *Biol Blood Marrow Transplant*
583 Hay BA, Abrams B, Zumbrunn AY, Valentine JJ, Warren LC, Petras SF, Shelly LD, Xia A, Varghese AH,
584 Hawkins JL, Van Camp JA, Robbins MD, Landschulz K, Harwood HJ, Jr. (2007) Aminopyrrolidineamide
585 inhibitors of site-1 protease. *Bioorg Med Chem Lett* 17: 4411-4
586 Haze K, Yoshida H, Yanagi H, Yura T, Mori K (1999) Mammalian transcription factor ATF6 is synthesized as a
587 transmembrane protein and activated by proteolysis in response to endoplasmic reticulum stress. *Mol Biol Cell*
588 10: 3787-99
589 Imperlini E, Gnecchi M, Rognoni P, Sabido E, Ciuffreda MC, Palladini G, Espadas G, Mancuso FM, Bozzola M,
590 Malpasso G, Valentini V, Palladini G, Orru S, Ferraro G, Milani P, Perlini S, Salvatore F, Merlini G, Lavatelli F
591 (2017) Proteotoxicity in cardiac amyloidosis: amyloidogenic light chains affect the levels of intracellular proteins
592 in human heart cells. *Sci Rep* 7: 15661
593 Jang I, Pottekat A, Poothong J, Yong J, Lagunas-Acosta J, Charbono A, Chen Z, Scheuner DL, Liu M, Itkin-
594 Ansari P, Arvan P, Kaufman RJ (2019) PDIA1/P4HB is required for efficient proinsulin maturation and ss cell
595 health in response to diet induced obesity. *Elife* 8
596 Kaplan B, Ramirez-Alvarado M, Sikkink L, Golderman S, Dispenzieri A, Livneh A, Gallo G (2009) Free light
597 chains in plasma of patients with light chain amyloidosis and non-amyloid light chain deposition disease. High
598 proportion and heterogeneity of disulfide-linked monoclonal free light chains as pathogenic features of amyloid
599 disease. *Br J Haematol* 144: 705-15
600 Kastritis E, Dialoupi I, Gavriatopoulou M, Roussou M, Kanellias N, Fotiou D, Ntanasis-Stathopoulos I,
601 Papadopoulou E, Ziogas DC, Stamatelopoulos K, Manios E, Ntalianis A, Eleutherakis-Papaiakovou E,
602 Papanikolaou A, Migkou M, Papanota AM, Gakiopoulou H, Psimenou E, Tselegkidi MI, Tsitsilonis O et al.
603 (2019) Primary treatment of light-chain amyloidosis with bortezomib, lenalidomide, and dexamethasone. *Blood*
604 *Adv* 3: 3002-3009
605 Kelly JW (2020) Pharmacologic Approaches for Adapting Proteostasis in the Secretory Pathway to Ameliorate
606 Protein Conformational Diseases. *Cold Spring Harb Perspect Biol* 12
607 Klimtchuk ES, Gursky O, Patel RS, Laporte KL, Connors LH, Skinner M, Seldin DC (2010) The critical role of
608 the constant region in thermal stability and aggregation of amyloidogenic immunoglobulin light chain.
609 *Biochemistry* 49: 9848-57
610 Koba H, Jin S, Imada N, Ishikawa T, Ninagawa S, Okada T, Sakuma T, Yamamoto T, Mori K (2020)
611 Reinvestigation of Disulfide-bonded Oligomeric Forms of the Unfolded Protein Response Transducer ATF6.
612 *Cell Struct Funct* 45: 9-21
613 Kroeger H, Grimsey N, Paxman R, Chiang WC, Plate L, Jones Y, Shaw PX, Trejo J, Tsang SH, Powers E,
614 Kelly JW, Wiseman RL, Lin JH (2018) The unfolded protein response regulator ATF6 promotes mesodermal
615 differentiation. *Sci Signal* 11
616 Lebeau P, Byun JH, Yousof T, Austin RC (2018) Pharmacologic inhibition of S1P attenuates ATF6 expression,
617 causes ER stress and contributes to apoptotic cell death. *Toxicol Appl Pharmacol* 349: 1-7
618 Lilie H, McLaughlin S, Freedman R, Buchner J (1994) Influence of protein disulfide isomerase (PDI) on
619 antibody folding in vitro. *J Biol Chem* 269: 14290-6
620 Manwani R, Hegenbart U, Mahmood S, Sachchithanantham S, Kyriakou C, Yong K, Popat R, Rabin N, Whelan
621 C, Dittrich T, Kimmich C, Hawkins P, Schonland S, Wechalekar A (2018) Deferred autologous stem cell
622 transplantation in systemic AL amyloidosis. *Blood Cancer J* 8: 101
623 Meier-Ewert HK, Sanchorawala V, Berk J, Finn KT, Skinner M, Seldin DC, Ruberg FL (2011) Regression of
624 cardiac wall thickness following chemotherapy and stem cell transplantation for light chain (AL) amyloidosis.
625 *Amyloid* 18 Suppl 1: 130-1

626 Merlini G, Comenzo RL, Seldin DC, Wechalekar A, Gertz MA (2014) Immunoglobulin light chain amyloidosis.
627 *Expert Rev Hematol* 7: 143-56
628 Merlini G, Dispenzieri A, Sanchorawala V, Schonland SO, Palladini G, Hawkins PN, Gertz MA (2018) Systemic
629 immunoglobulin light chain amyloidosis. *Nat Rev Dis Primers* 4: 38
630 Milani P, Palladini G, Merlini G (2018) New concepts in the treatment and diagnosis of amyloidosis. *Expert Rev*
631 *Hematol* 11: 117-127
632 Nadanaka S, Okada T, Yoshida H, Mori K (2007) Role of disulfide bridges formed in the luminal domain of
633 ATF6 in sensing endoplasmic reticulum stress. *Mol Cell Biol* 27: 1027-43
634 Nadanaka S, Yoshida H, Mori K (2006) Reduction of disulfide bridges in the lumenal domain of ATF6 in
635 response to glucose starvation. *Cell Struct Funct* 31: 127-34
636 Nikesitch N, Lee JM, Ling S, Roberts TL (2018) Endoplasmic reticulum stress in the development of multiple
637 myeloma and drug resistance. *Clin Transl Immunology* 7: e1007
638 Obeng EA, Carlson LM, Gutman DM, Harrington WJ, Jr., Lee KP, Boise LH (2006) Proteasome inhibitors
639 induce a terminal unfolded protein response in multiple myeloma cells. *Blood* 107: 4907-16
640 Oka OB, van Lith M, Rudolf J, Tungkum W, Pringle MA, Bulleid NJ (2019) ERp18 regulates activation of
641 ATF6alpha during unfolded protein response. *EMBO J* 38: e100990
642 Palladini G, Hegenbart U, Milani P, Kimmich C, Foli A, Ho AD, Vidus Rosin M, Albertini R, Moratti R, Merlini G,
643 Schonland S (2014) A staging system for renal outcome and early markers of renal response to chemotherapy
644 in AL amyloidosis. *Blood* 124: 2325-32
645 Paxman R, Plate L, Blackwood EA, Glembotski C, Powers ET, Wiseman RL, Kelly JW (2018) Pharmacologic
646 ATF6 activating compounds are metabolically activated to selectively modify endoplasmic reticulum proteins.
647 *Elife* 7
648 Pinney JH, Smith CJ, Taube JB, Lachmann HJ, Venner CP, Gibbs SD, Dungu J, Banypersad SM, Wechalekar
649 AD, Whelan CJ, Hawkins PN, Gillmore JD (2013) Systemic amyloidosis in England: an epidemiological study.
650 *Br J Haematol* 161: 525-32
651 Plate L, Cooley CB, Chen JJ, Paxman RJ, Gallagher CM, Madoux F, Genereux JC, Dobbs W, Garza D, Spicer
652 TP, Scampavia L, Brown SJ, Rosen H, Powers ET, Walter P, Hodder P, Wiseman RL, Kelly JW (2016) Small
653 molecule proteostasis regulators that reprogram the ER to reduce extracellular protein aggregation. *Elife* 5
654 Plate L, Rius B, Nguyen B, Genereux JC, Kelly JW, Wiseman RL (2019) Quantitative Interactome Proteomics
655 Reveals a Molecular Basis for ATF6-Dependent Regulation of a Destabilized Amyloidogenic Protein. *Cell*
656 *Chem Biol* 26: 913-925 e4
657 Plate L, Wiseman RL (2017) Regulating Secretory Proteostasis through the Unfolded Protein Response: From
658 Function to Therapy. *Trends Cell Biol* 27: 722-737
659 Powers ET, Morimoto RI, Dillin A, Kelly JW, Balch WE (2009) Biological and chemical approaches to diseases
660 of proteostasis deficiency. *Annu Rev Biochem* 78: 959-91
661 Ramirez-Alvarado M (2012) Amyloid formation in light chain amyloidosis. *Curr Top Med Chem* 12: 2523-33
662 Ri M (2016) Endoplasmic-reticulum stress pathway-associated mechanisms of action of proteasome inhibitors
663 in multiple myeloma. *Int J Hematol* 104: 273-80
664 Salinaro F, Meier-Ewert HK, Miller EJ, Pandey S, Sanchorawala V, Berk JL, Seldin DC, Ruberg FL (2017)
665 Longitudinal systolic strain, cardiac function improvement, and survival following treatment of light-chain (AL)
666 cardiac amyloidosis. *Eur Heart J Cardiovasc Imaging* 18: 1057-1064
667 Shi J, Guan J, Jiang B, Brenner DA, Del Monte F, Ward JE, Connors LH, Sawyer DB, Semigran MJ,
668 Macgillivray TE, Seldin DC, Falk R, Liao R (2010) Amyloidogenic light chains induce cardiomyocyte contractile
669 dysfunction and apoptosis via a non-canonical p38alpha MAPK pathway. *Proc Natl Acad Sci U S A* 107: 4188-
670 93
671 Shoulders MD, Ryno LM, Genereux JC, Moresco JJ, Tu PG, Wu C, Yates JR, 3rd, Su AI, Kelly JW, Wiseman
672 RL (2013) Stress-independent activation of XBP1s and/or ATF6 reveals three functionally diverse ER
673 proteostasis environments. *Cell Rep* 3: 1279-92
674 Sidrauski C, Acosta-Alvear D, Khoutorsky A, Vedantham P, Hearn BR, Li H, Gamache K, Gallagher CM, Ang
675 KK, Wilson C, Okreglak V, Ashkenazi A, Hann B, Nader K, Arkin MR, Renslo AR, Sonenberg N, Walter P
676 (2013) Pharmacological brake-release of mRNA translation enhances cognitive memory. *Elife* 2: e00498
677 Sidrauski C, McGeachy AM, Ingolia NT, Walter P (2015) The small molecule ISRIB reverses the effects of
678 eIF2alpha phosphorylation on translation and stress granule assembly. *Elife* 4
679 Sikkink LA, Ramirez-Alvarado M (2010) Cytotoxicity of amyloidogenic immunoglobulin light chains in cell
680 culture. *Cell Death Dis* 1: e98

681 Sorensen S, Ranheim T, Bakken KS, Leren TP, Kulseth MA (2006) Retention of mutant low density lipoprotein
682 receptor in endoplasmic reticulum (ER) leads to ER stress. *J Biol Chem* 281: 468-76
683 Sun Z, Brodsky JL (2019) Protein quality control in the secretory pathway. *J Cell Biol* 218: 3171-3187
684 Torres SE, Gallagher CM, Plate L, Gupta M, Liem CR, Guo X, Tian R, Stroud RM, Kampmann M, Weissman
685 JS, Walter P (2019) Ceapins block the unfolded protein response sensor ATF6alpha by inducing a neomorphic
686 inter-organelle tether. *Elife* 8
687 Wang L, Wang X, Wang CC (2015) Protein disulfide-isomerase, a folding catalyst and a redox-regulated
688 chaperone. *Free Radic Biol Med* 83: 305-13
689 Wechalekar AD, Schonland SO, Kastritis E, Gillmore JD, Dimopoulos MA, Lane T, Foli A, Foard D, Milani P,
690 Rannigan L, Hegenbart U, Hawkins PN, Merlini G, Palladini G (2013) A European collaborative study of
691 treatment outcomes in 346 patients with cardiac stage III AL amyloidosis. *Blood* 121: 3420-7
692 Ye J, Rawson RB, Komuro R, Chen X, Dave UP, Prywes R, Brown MS, Goldstein JL (2000) ER stress induces
693 cleavage of membrane-bound ATF6 by the same proteases that process SREBPs. *Mol Cell* 6: 1355-64
694

695

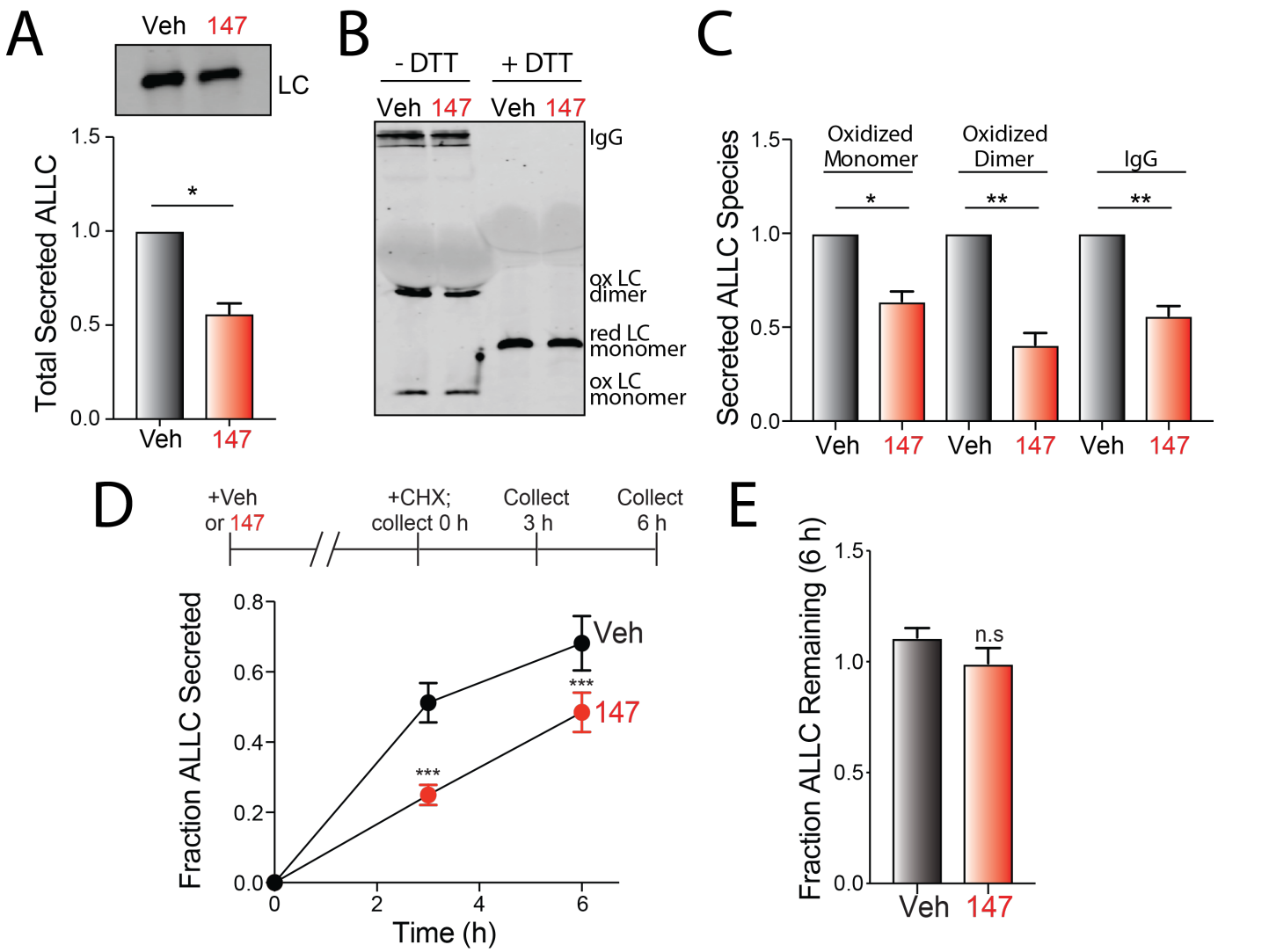

Figure 1 (with 1 supplement). Compound 147 reduces secretion of ALLC from AL patient derived ALMC-2 cells.

- **A.** Representative immunoblot and quantification of ALLC in conditioned media prepared on ALMC-2 cells treated for 18 hr with vehicle or **147** (10 μM). Error bars show SEM for n= 4 independent experiments. *p<0.05 for a paired t-test.
- **B.** Representative non-reducing (-DTT) and reducing (+DTT) immunoblots of conditioned media prepared on ALMC-2 cells treated for 18 hr with vehicle or **147** (10 μM). The fully-assembled IgGs, oxidized LC dimers, oxidized LC monomers, and reduced LC monomers are indicated.
- **C.** Quantification of non-reducing immunoblots as shown in **Figure 1B** showing the relative recovery of oxidized LC monomers, oxidized LC dimers, and fully-assembled IgGs. Error bars show SEM for n=3 or 4 independent experiments. **p<0.05, **p<0.01 from a paired t-test.
- **D.** Graph showing the fraction ALLC secreted from ALMC-2 cells treated with vehicle or **147** (10 μM) for 18 hr and then treated with cycloheximide (CHX; 50 μg/mL) at 0, 3 or 6 h. ALLC in conditioned media and lysates were measured by ELISA. The experimental protocol is shown above. Fraction secreted was calculated using: [fraction secreted = ALLC in media at t= 3 or 6 h / ALLC in the lysate at t=0 h]. Error bars show SEM for n=5 replicates. ***p<0.005 vs Veh from an unpaired t-test.
- **E.** Graph showing the fraction ALLC remaining from ALMC-2 cells treated for 18 h with vehicle or **147** (10 μM) and then treated with cycloheximide (CHX; 50 μg/mL), as in **Figure 1D**. ALLC in conditioned media and lysates were measured by ELISA. Fraction ALLC remaining was calculated using: [fraction ALLC remaining = (ALLC in media t=6 h + ALLC in lysate at t=6h) / ALLC in lysate at t = 0 h]. Error bars show SEM for n= 5 replicates. (n.s), not significant.

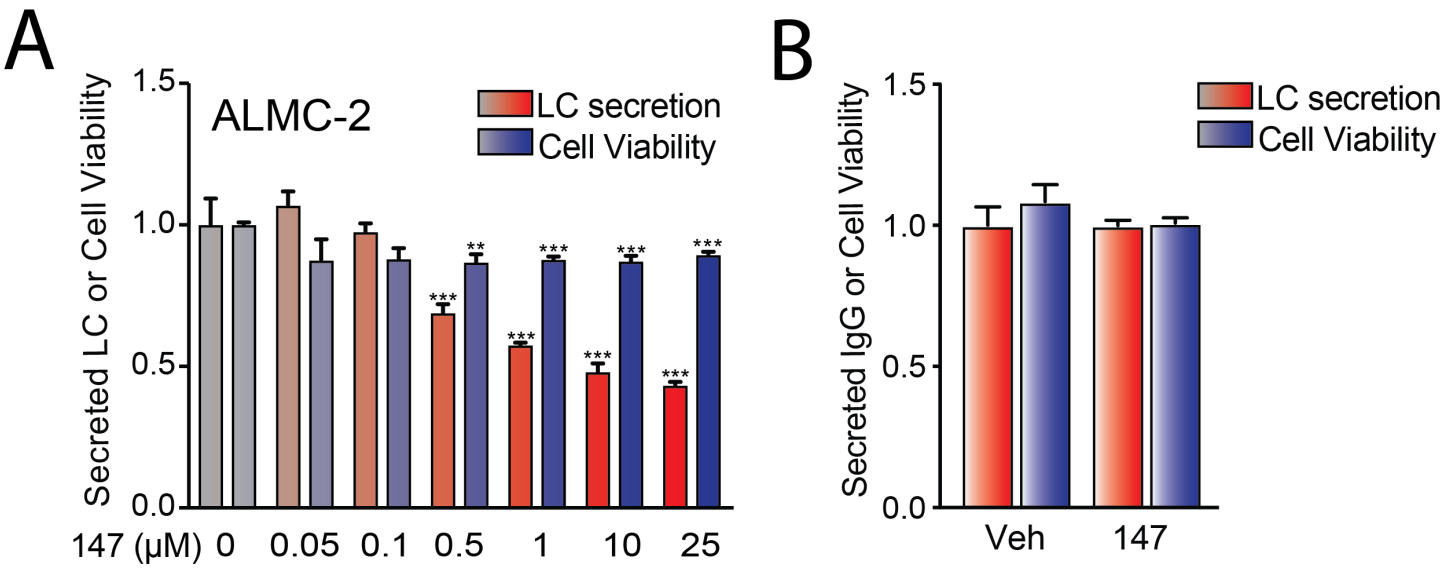

Figure 1 – figure supplement 1. Compound 147 reduces secretion of ALLC from AL patient derived ALMC-2 cells.

A. Graphs showing relative ALLC in conditioned media measured by ELISA (red) and cellular viability measured by CellTiter-Glo (blue) in ALMC-2 cells treated for 18 hr with vehicle or **147** (10 μM). Error bars show SEM for n= 4 replicates. ***p<0.005 vs Veh from an unpaired t-test.

B. Graph showing relative media levels of IgG measured by ELISA (red) and cellular viability measured by CellTiter-Glo (blue) in KAS-6/1 cells treated with vehicle or **147** (10 μM) for 18 hr. Error bars show SEM for n = 5 replicates. ***p<0.005 vs Veh from an unpaired t-test.

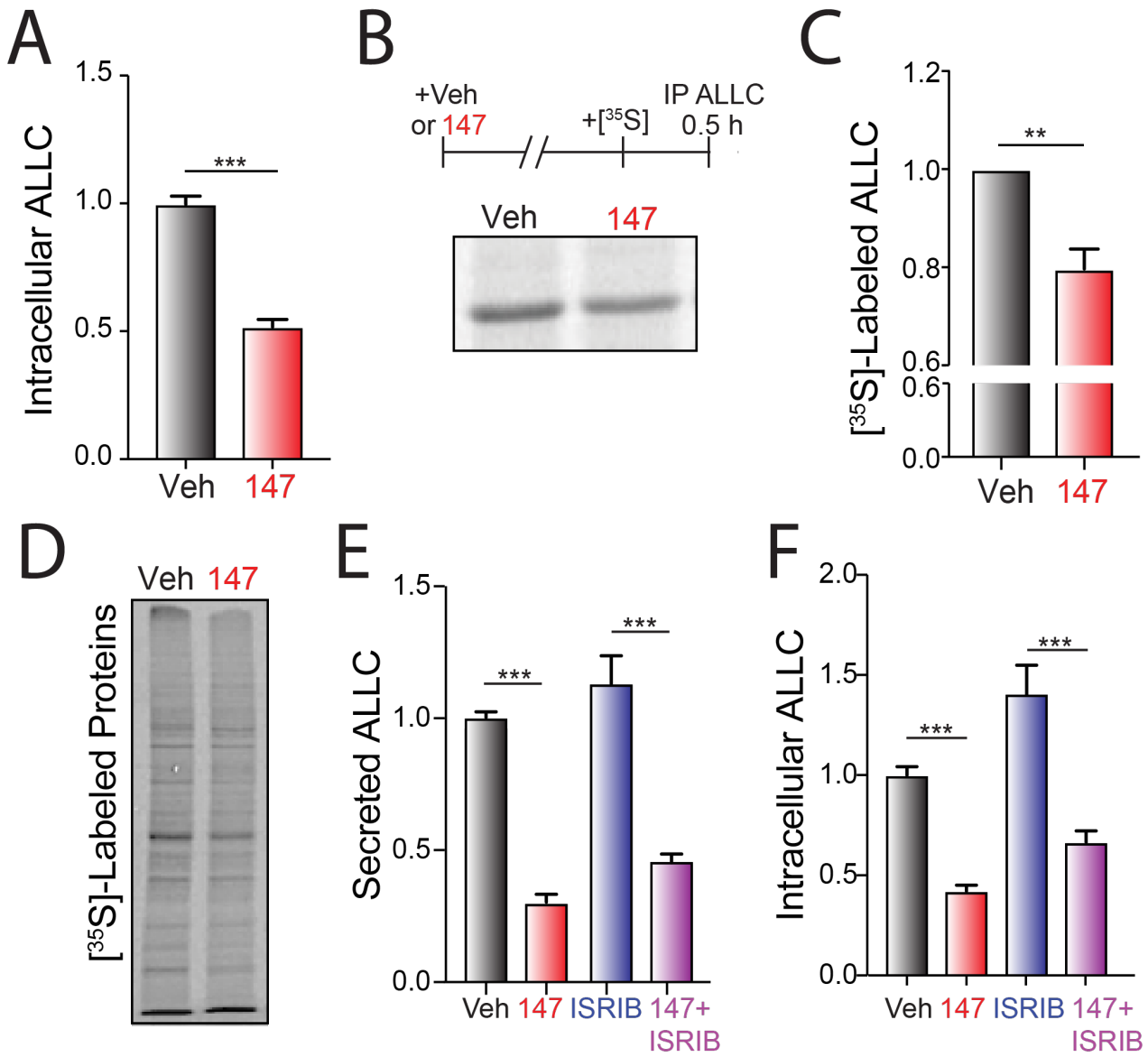

Figure 2 (with 1 supplement). Compound 147 reduces lysate levels of ALLC in ALMC-2 cells.

A. Graph showing normalized amounts of ALLC in lysates prepared from ALMC-2 cells incubated for 18 hr with vehicle or **147** (10 μM). ALLC was quantified by ELISA. Error bars show SEM for n= 23 replicates across five independent experiments. ***p<0.005 from an unpaired t-test.

B. Representative autoradiogram of [^{35}S]-labeled ALLC immunopurified from ALMC-2 cells treated for 18 hr with vehicle or **147** (10 μM) and then labeled for 30 min with [^{35}S]. The experimental protocol is shown above.

C. ALLC quantification of autoradiograms shown in **Figure 2B** normalized to Veh-treated cells. Error bars show SEM for n= 5 independent experiments. **p<0.01 from a paired t-test.

D. Autoradiogram of whole cell lysates prepared from ALMC-2 cells treated for 18 hr with vehicle or **147** and then metabolically labeled with [^{35}S] for 30 min.

E. Quantification of ALLC in conditioned media prepared on ALMC-2 cells treated for 18 hr with vehicle, **147** (10 μM), and/or ISRIB (200 nM), as indicated. ALLC was measured by ELISA and normalized to vehicle-treated cells. Error bars show SEM for n = 14 replicates across three independent experiments. ***p<0.005 from an unpaired t-test.

F. Quantification of ALLC in lysates prepared from ALMC-2 cells treated for 18 hr with vehicle, **147** (10 μM), and/or ISRIB (200 nM), as indicated. ALLC was measured by ELISA and normalized to vehicle-treated cells. Error bars show SEM for n = 14 replicates across three independent experiments. ***p<0.005 from an unpaired t-test.

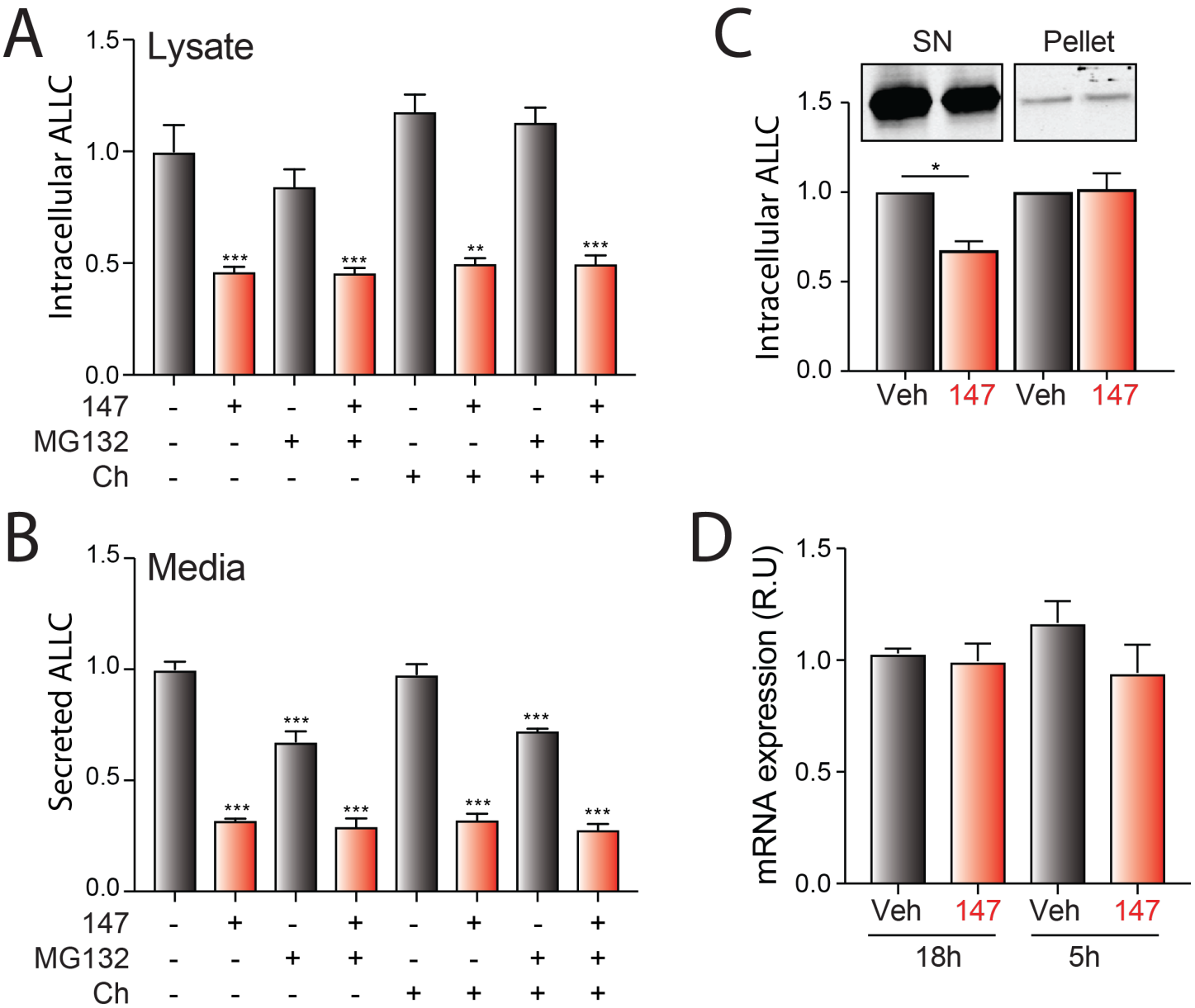

Figure 2 – figure supplement 1. Compound 147 reduces lysate levels of ALLC in ALMC-2 cells.

A. Bar graphs showing normalized amounts of ALLC in lysates prepared from ALMC-2 cells treated for 18 hr with vehicle or **147** (10 μM). MG132 (10 μM) or chloroquine (Ch, 20 μM) were added as indicated for the last 5 hours of this incubation and during the 2 hours of media conditioning. ALLC was quantified by ELISA. Error bars show SEM for n=5 replicates. *** $p<0.005$ vs Veh from an unpaired t-test.

B. Bar graphs showing normalized amounts of ALLC in conditioned media prepared from ALMC-2 cells treated for 18 hr with Veh, **147** (10 μM). MG132 (10 μM) or chloroquine (20 μM) were added for the last 5 hours of this incubation and during the 2 hours of media conditioning. ALLC was quantified by ELISA. Error bars show SEM for n=5 replicates. *** $p<0.005$ vs Veh from an unpaired t-test.

C. Representative immunoblot and normalized quantification of ALLC in fractionated lysates from ALMC-2 cells treated with Veh or **147** (10 μM) for 18 hr. The supernatant fraction (SN) is the soluble protein fraction obtained after lysing with RIPA buffer (no DTT). Pellets derived from the first lysis were then solubilized by treatment with SDS (2%), DTT and sonication. Error bars show SEM for n=3 independent replicates. *$p<0.05$ from a paired t-test

D. Bar graphs showing ALLC mRNA measured by qPCR in ALMC-2 cells treated with vehicle or **147** for 18 hr or 5 hr. Error bars show 95% confident intervals for n=3 replicates.

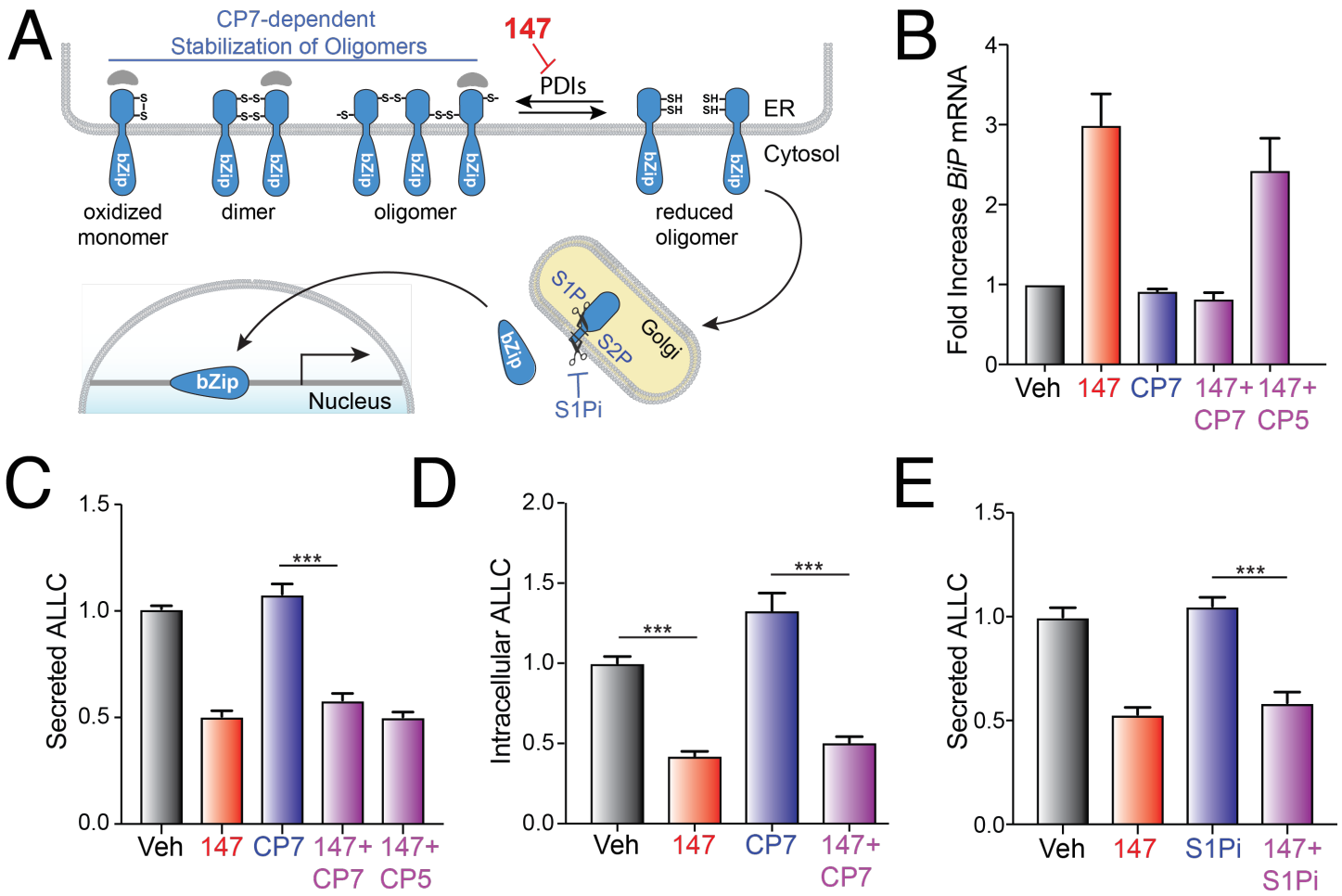

Figure 3 (with 1 supplement). 147-dependent reductions in ALLC secretion are independent of ATF6 activation.

A. Illustration showing the mechanism of **147**-dependent ATF6 activation. ATF6 is retained within the ER as oxidized monomers, disulfide-bonded dimers, or disulfide-bonded oligomers that are maintained by PDIs. Compound **147** covalently modifies a subset of PDIs, increasing the population of reduced ATF6 monomers that can traffic to the Golgi and undergo proteolytic processing by S1P and S2P. This releases the N-terminal bZIP domain of ATF6 to localize to the nucleus and promote ATF6 transcriptional signaling. The specific steps of this activation mechanism inhibited by CP7 or S1Pi are shown.

B. Graph showing *BiP* expression measured by qPCR in ALMC-2 cells treated for 5 hr with vehicle or **147** (10 μM), CP7 (10 μM), or CP5 (10 μM), as indicated. Error bars show 95% confidence interval for n = 3 replicates.

C. Bar graphs showing normalized amounts of ALLC in conditioned media prepared from ALMC-2 cells treated for 18 hr with vehicle or **147** (10 μM), CP7 (10 μM), or CP5 (10 μM), as indicated. ALLC was quantified by ELISA. Error bars show SEM for n=21 replicates across four independent experiments. ***p<0.005 from an unpaired t-test.

D. Bar graphs showing normalized amounts of ALLC in in lysates prepared from ALMC-2 cells treated for 18 hr with vehicle, **147** (10 μM) and/or CP7 (10 μM), as indicated. ALLC was quantified by ELISA. Error bars show SEM for n=10 replicates across two independent experiments. ***p<0.005 from an unpaired t-test.

E. Bar graphs showing normalized amounts of ALLC in conditioned media from ALMC-2 cells treated for 18 hr with vehicle or **147** (10 μM) and/or the site 1 protease inhibitor PF429242 (S1Pi; 10 μM), as indicated. ALLC was quantified by ELISA. Error bars show SEM for n=8 replicates across two independent experiments. ***p<0.005 from an unpaired t-test.

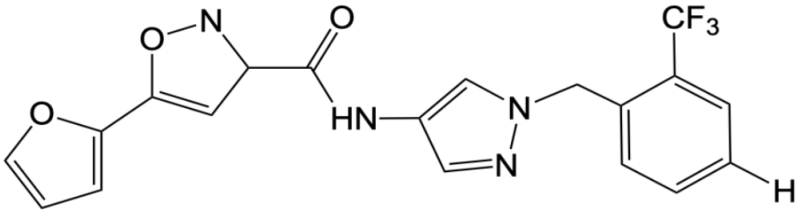

CP7

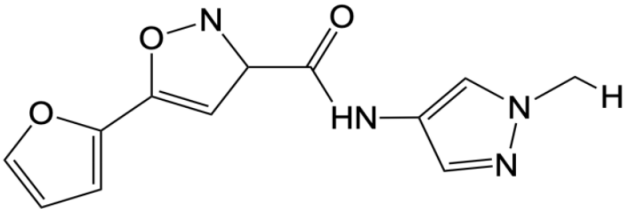

CP5

Figure 3 – figure supplement 1. 147-Dependent Reductions in ALLC Secretion are Independent of ATF6 Activation. Chemical structures of the ATF6 inhibitor CP7 and its inactive analog CP5 (Gallagher et al., 2016, Gallagher & Walter, 2016).

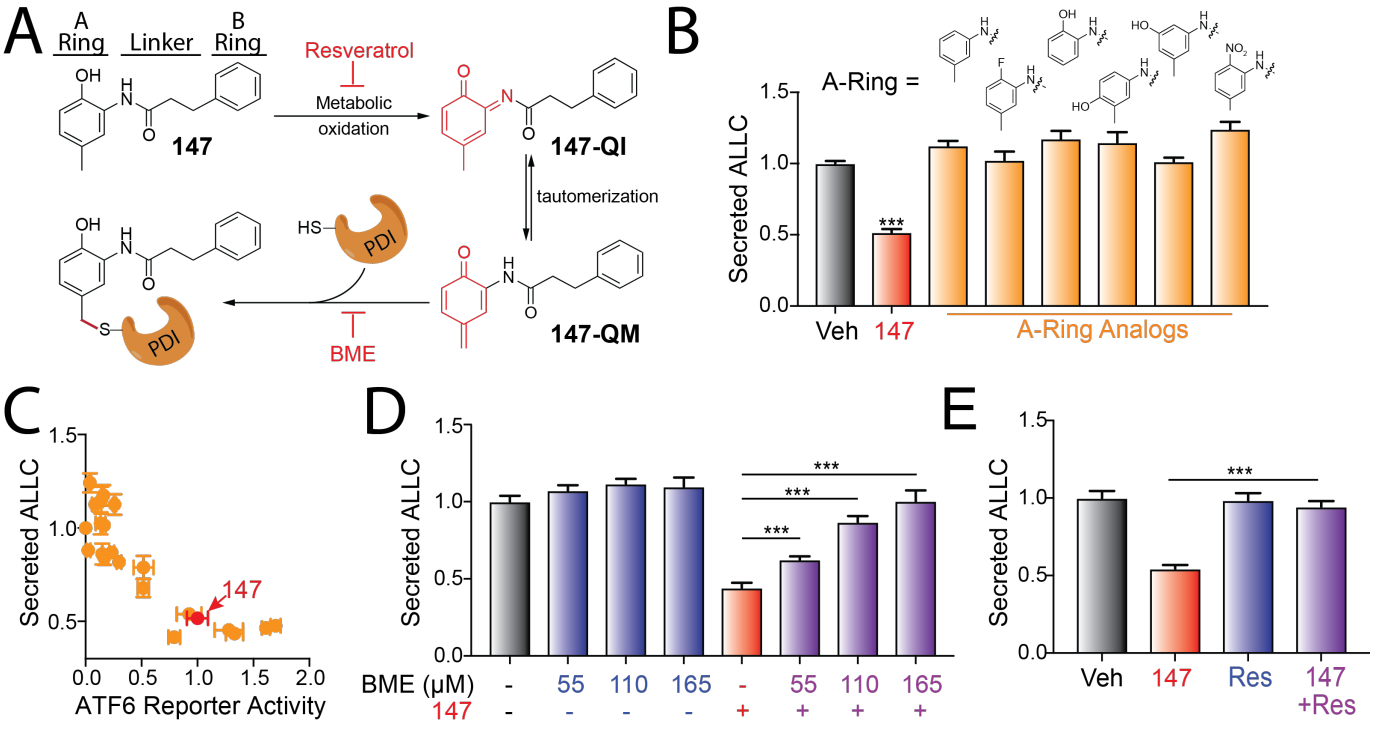

Figure 4 (with 1 supplement). Compound 147 reduces ALLC secretion through a mechanism involving compound metabolic activation and covalent protein modification.

A. Illustration showing the metabolic activation of **147** to a quinone imide (**147-QI**) and quinone methide (**147-QM**). These reactive electrophiles covalently modify ER proteins including multiple PDIs. The 'A'-ring, linker, and 'B'-ring of **147** are indicated. Specific steps inhibited by resveratrol and β-mercaptoethanol (BME) are also indicated. Adapted from (Paxman et al., 2018).

B. Graph showing normalized amounts of ALLC in conditioned media from ALMC-2 cells treated for 18 hr with vehicle, **147** (10 μM) or the indicated **147** 'A'-ring analog (10 μM). ALLC was quantified by ELISA. Error bars show SEM for n=10 replicates across two independent experiments. ***p<0.005 vs Veh from an unpaired t-test.

C. Plot comparing the normalized activation of an ATF6-selective luciferase reporter in HEK293 cells (Paxman et al., 2018) to reductions in ALLC secretion from ALMC-2 cells for **147** (10 μM) or **147** analogs containing alterations to the 'A'-ring, linker, and 'B'-ring. Error bars for the ATF6 reporter activation show SEM for n=3 independent experiments. Error bars for ALLC secretion show n=10 replicates across two independent experiments.

D. Graph showing normalized amounts of ALLC secretion from ALMC-2 cells treated for 18 hr with vehicle or **147** (10 μM) and/or β mercaptethanol (BME), as indicated. ALLC was quantified by ELISA. Error bars show SEM for n=10 replicates across two independent experiments. *** p<0.005 from a paired t-test.

E. Graph showing normalized ALLC secretion from ALMC-2 cells treated for 18 hr with vehicle, **147** (10 μM) and/or resveratrol (Res, 10 μM), as indicated. ALLC was quantified by ELISA. Error bars show SEM for n=9 replicates across two independent experiments. *** p<0.005 from a paired t-test.

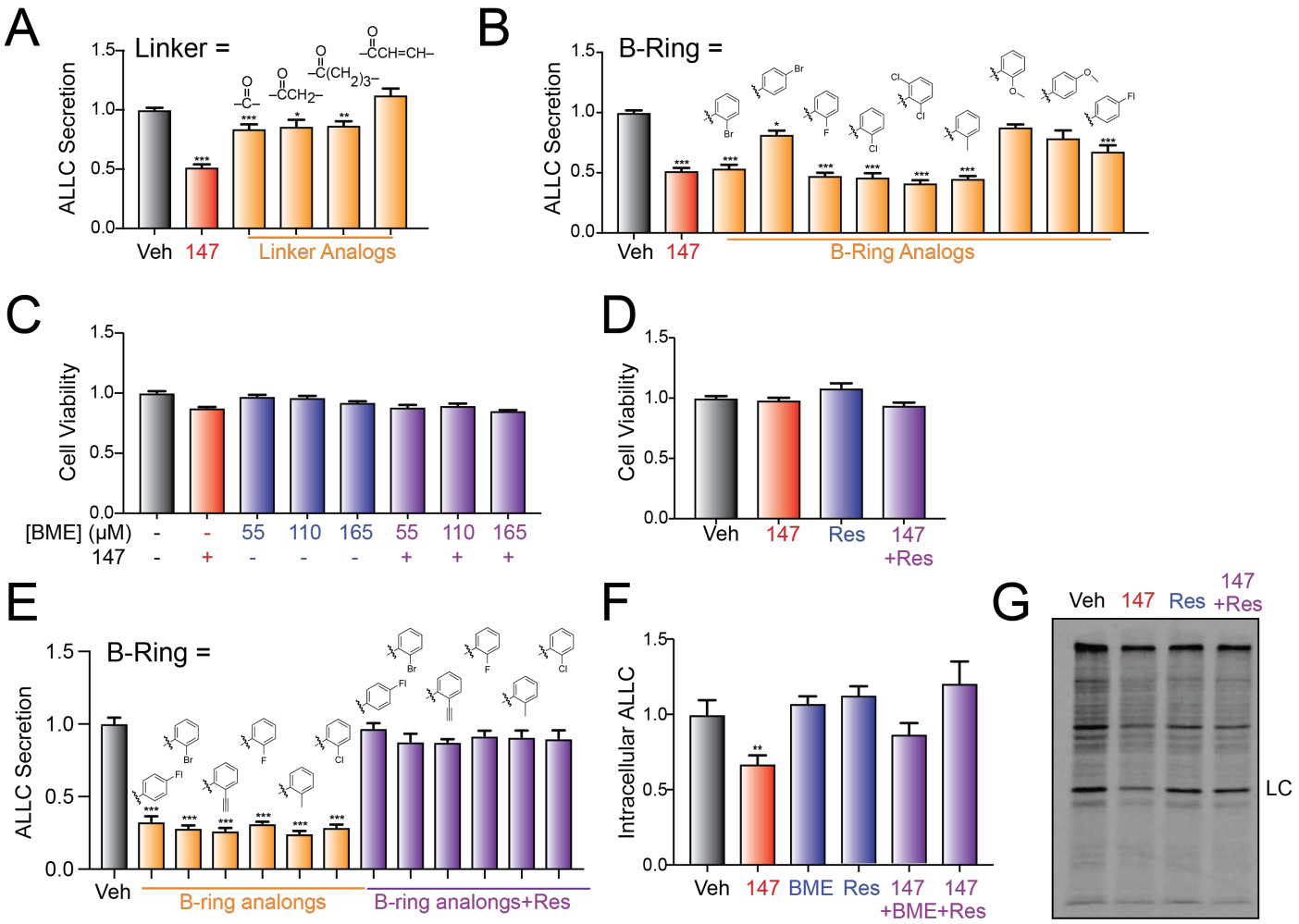

Figure 4 – figure supplement 1. Compound 147 reduces ALLC secretion through a mechanism involving compound metabolic activation and covalent protein modification.

A. Graph showing normalized ALLC in conditioned media from ALMC-2 cells treated for 18 hr with vehicle, **147** (10 μM) or the indicated **147** 'Linker'-analog (10 μM). ALLC was quantified by ELISA. Error bars show SEM for n=10 replicates across two independent experiments. *p< 0.05, **p<0.01, ***p<0.005 vs Veh from an unpaired t-test.

B. Graph showing normalized ALLC in conditioned media from ALMC-2 cells treated for 18 hr with vehicle, **147** (10 μM) or the indicated **147** 'B' ring'-analog (10 μM). ALLC was quantified by ELISA. Error bars show SEM for n=10 replicates across two independent experiments. *p< 0.05, **p<0.01, ***p<0.005 vs Veh from an unpaired t-test.

C. Graph showing normalized quantification of cell viability measured with CellTiter-Glo of ALMC-2 cells treated with vehicle, **147** (10 μM) and/or β-mercaptoethanol (BME) for 18 hr. Error bars show SEM for n=5 replicates..

D. Graph showing normalized quantification of cell viability measured with CellTiter-Glo of ALMC-2 cells treated with vehicle, **147** (10 μM) and/or resveratrol (Res: 10 μM) for 18 hr. Error bars show SEM for n=10 replicates across two independent experiments.

E. Graph showing normalized ALLC in conditioned media from ALMC-2 cells treated for 18 hr with vehicle, **147** (10 μM) or 'B ring'-analog (10 μM) with or without resveratrol (10 μM). Error bars show SEM for n>3 replicates. ***p<0.005 vs Veh from an unpaired t-test.

F. Graph showing the normalized amounts of ALLC in lysates prepared from ALMC-2 cells treated for 18 hr with vehicle, **147** (10 μM), resveratrol (10 μM), or β-mercaptoethanol (BME: 165 μM), as indicated. ALLC was quantified by ELISA. Error bars show SEM shows n=5 replicates. **p<0.01 vs Veh from an unpaired t-test.

G. Representative autoradiogram of whole cell lysates prepared from ALMC-2 cells treated for 18 hr with vehicle, **147** and/or resveratrol (10 μM) and then metabolically labeled with [^{35}S] for 30 min.

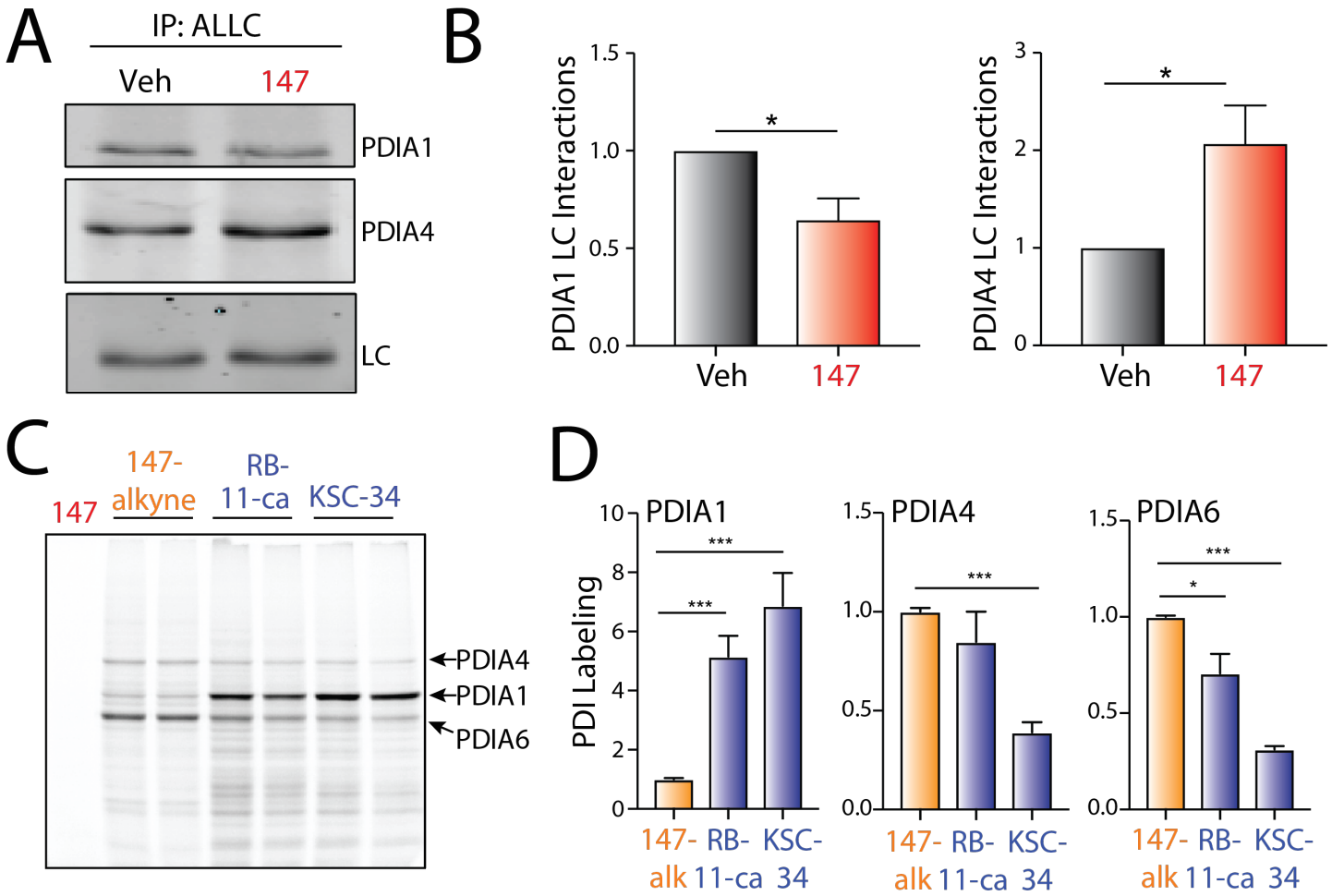

Figure 5 (with 1 supplement). PDI interactions with ALLC are disrupted by 147 treatment.

A. Representative immunoblot of PDIA1 and PDIA4 in ALLC immunopurifications from ALMC-2 cells treated for 5 hr with vehicle or **147** (10 μM). Inputs from this experiment are shown in **Figure 5 – figure supplement 1E**.

B. Quantification of PDIA1 and PDIA4 from immunoblots as shown in **Figure 5A**. The recovery of each PDI was normalized to the recovery of ALLC under each condition, allowing accurate evaluation of the interaction between these two proteins. Error bars show SEM for n>5 independent experiments. *p< 0.05 for paired t-tests.

C. Representative fluorescence gel showing the covalent modification of proteins in ALMC-2 cells treated for 18 hr with **147-alkyne** (10 μM), RB-11-ca (30 μM), or KSC-34 (30 μM). Click chemistry was used to incorporate a TAMRA fluorophore onto the alkyne contained in each of these molecules. Cells treated with **147** are shown as a control. The PDI bands were assigned based on previous mass spectrometric analysis of SDS-PAGE bands excised from identical gels of **147-alkyne** treated ALMC-2 cell lysates (Paxman et al., 2018).

D. Normalized quantification of PDIA1, PDIA4, and PDIA6 labeling from gels as shown in **Figure 5C**. Error bars show SEM for n=4 replicates across two independent experiments. *p< 0.05, **p<0.01, ***p<0.005 for paired t-tests.

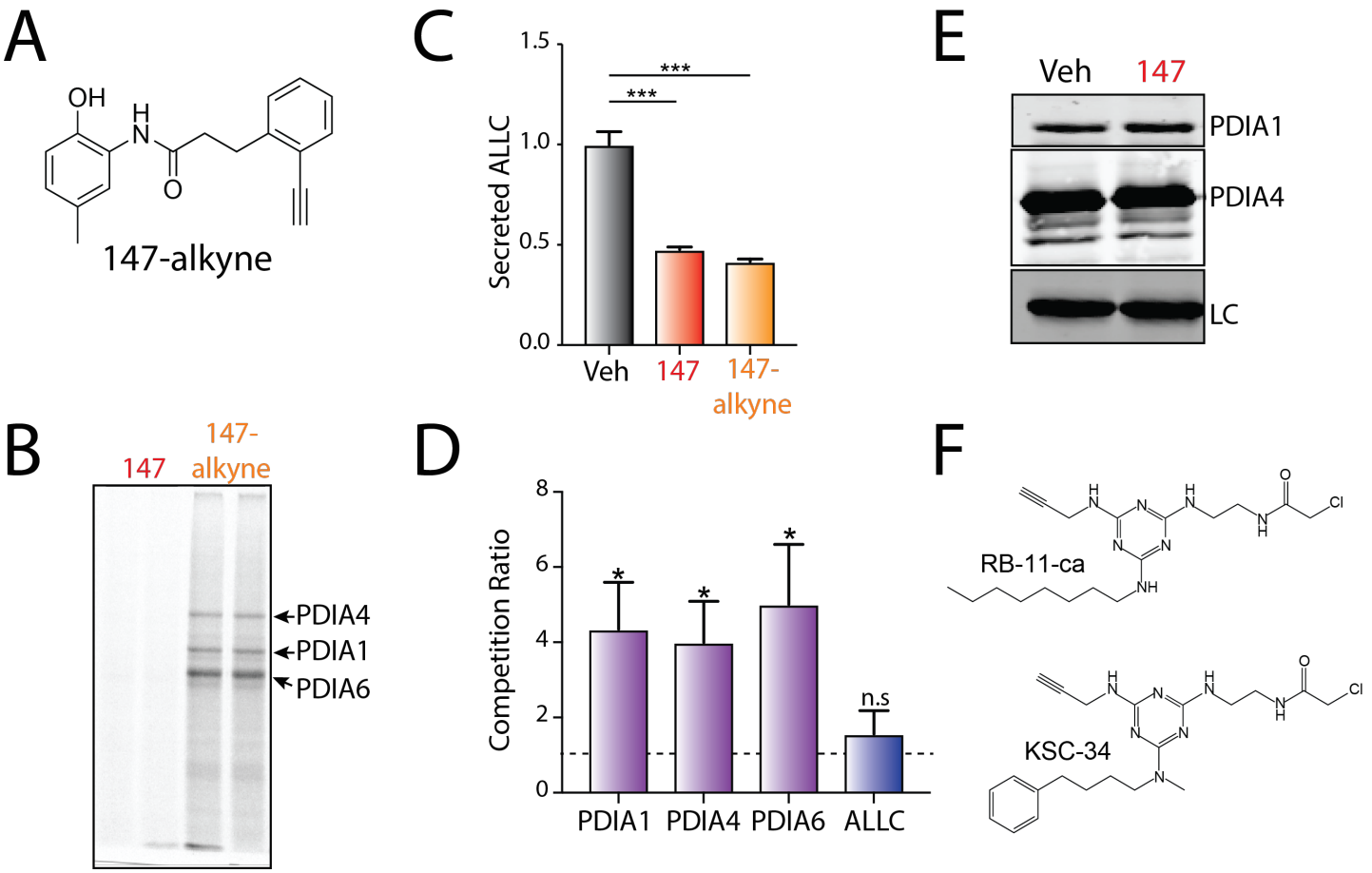

Figure 5 – figure supplement 1. PDI interactions with ALLC are disrupted by 147 treatment.

- **A.** Chemical structure of **147-alkyne**.
- **B.** Representative gel showing the covalent modification of proteins in ALMC-2 cells treated for 18 hr with **147** (10 μM) or **147-alkyne** (10 μM). Click chemistry was used to incorporate a TAMRA fluorophore onto the alkyne contained in each of these molecules. Cells treated with **147** are shown as a control. The PDI bands were assigned based on previous mass spectrometric analysis of SDS-PAGE bands excised from identical gels of **147-alkyne** treated ALMC-2 cell lysates (Paxman et al., 2018).
- **C.** Graph showing ALLC secreted from ALMC-2 cells treated for 18 hr with vehicle, **147** (10 μM) or **147-alkyne** (10 μM). Error bars show SEM for n=10 replicates across two independent experiments. ***p<0.005 from an unpaired t-test.
- **D.** Graph showing competition ratio of the indicated PDI or ALLC in affinity purifications isolated from ALMC-2 cells treated for 18 h with **147-alkyne** (10 μM) or **147-alkyne** (10 μM) and an excess of **147** (50 μM). These data are from experiments described in (Paxman et al., 2018). Briefly, after incubation with ALMC-2 cells, **147-alkyne** was modified with a biotin allowing isolation of the proteins covalently modified by **147-alkyne** using streptavidin affinity purification. The recovery of different proteins across conditions was then quantified using tandem mass tag (TMT) labeling and multi-dimensional protein identification technology (MuDPIT). The competition ratio was calculated as previously described using the equation: competition ratio = protein signal from cells treated with **147-alkyne** treated / protein signal from cells treated with **147-alkyne** and excess **147** (Paxman et al., 2018). Error bars show SEM for n=4 paired replicates across two independent experiments. *p<0.05 from a paired t-test. (n.s), not significant.
- **E.** Immunoblot showing lysate levels of PDIA1, PDIA4 and ALLC in ALMC-2 cells treated for 5 hr with vehicle or **147** (10 μM). These are inputs from the immunopurifications shown in **Figure 5A**.
- **F.** Chemical structures of the PDI inhibitors RB-11-ca and KSC-34.

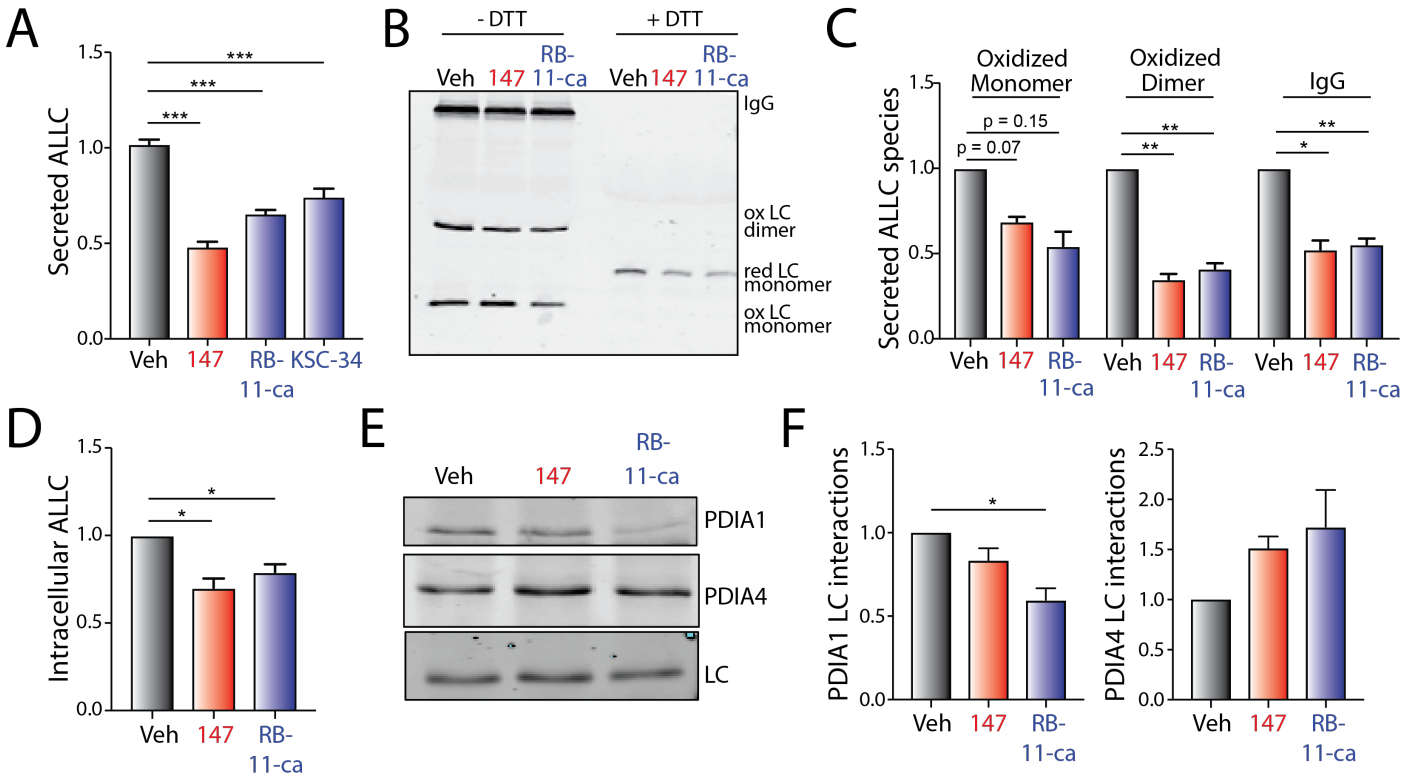

Figure 6 (with 1 supplement). Pharmacologic targeting of PDIs reduces ALLC secretion from ALMC-2 cells

A. Graph showing normalized ALLC secretion from ALMC-2 cells treated for 18 hr with vehicle, **147** (10 μM), RB-11-CA (30 μM), or KSC-34 (30 μM). ALLC was quantified by ELISA. Error bars show SEM for n>9 replicates across >two independent experiments. ***p<0.005 from an unpaired t-test.

B. Representative non-reducing (-DTT) and reducing (+DTT) immunoblots of conditioned media prepared from ALMC-2 cells treated for 18 hr with vehicle, **147** (10 μM) or RB-11-ca (30 μM). The fully-assembled IgGs, oxidized LC dimers, oxidized LC monomers, and reduced LC monomers are indicated.

C. Graph showing normalized quantification of non-reducing immunoblots as shown in **Figure 6B** for oxidized LC monomers, oxidized LC dimers, and fully-assembled IgGs. Error bars show SEM for n>2 independent experiments. *p<0.05, **p<0.01 from a paired t-test.

D. Graph showing normalized quantification of ALLC in lysates prepared from ALMC-2 cells treated for 18 hr with vehicle, **147** (10 μM) or RB-11-ca (30 μM). ALLC was measured by immunoblotting**.** Error bars show SEM for n=4 independent experiments. *p<0.05 from a paired t-test.

E. Representative immunoblot of ALLC immunopurified from ALMC-2 cells treated for 5 hr with vehicle, **147** (10 μM) or RB-11-ca (30 μM).

F. Normalized quantification of PDIA1 and PDIA4 from immunoblots as shown in **Figure 6E**. The recovery of each PDI was normalized to the recovery of ALLC under each condition, allowing accurate evaluation of the interaction between these two proteins. Error bars show SEM for n>2 independent experiments. *p< 0.05 from a paired t-test.

933

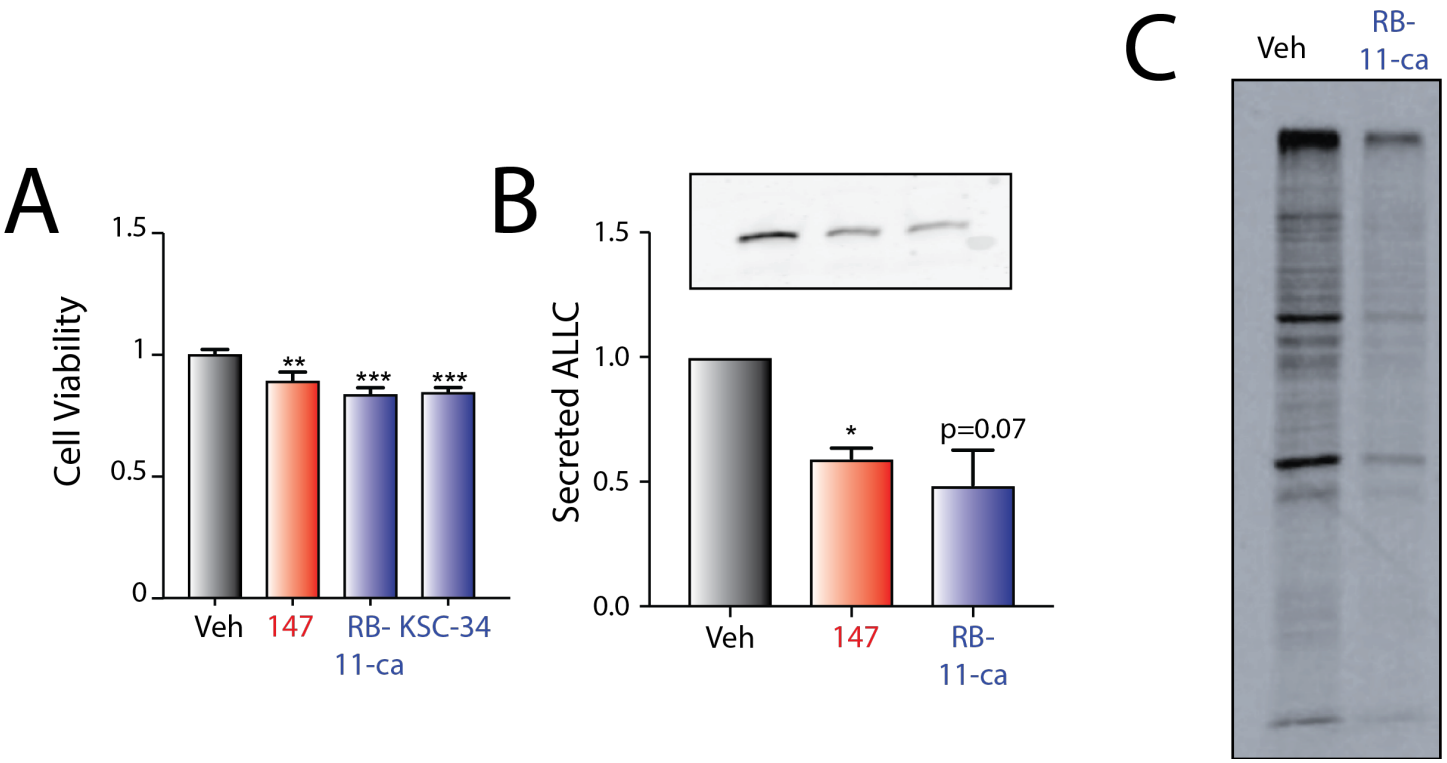

934
935
936 **Figure 6 – figure supplement 1. Pharmacologic targeting of PDIs reduces ALLC secretion from ALMC-2**
937 **cells**
938 **A.** Graph showing the viability measured by CellTiter Glo for ALMC-2 cells treated for 18 hr with vehicle,
939 **147** (10 μM), RB-11-ca (30 μM), or KSC-34 (30 μM). ALLC was quantified by ELISA. Error bars show
940 SEM for n=11 replicates across 2 independent experiments. ***p<0.005 vs Veh from an unpaired t-test.
941 **B.** Representative immunoblot and quantification of ALLC in conditioned media prepared from ALMC-2
942 cells treated with vehicle, **147** (10 μM) or Rb-11-ca (30 μM) for 18 h. Error bars show SEM for n=3
943 independent experiments. *p<0.05 vs Veh from a one-tailed paired t-test.
944 **C.** Representative autoradiogram of whole cell lysates prepared from ALMC-2 cells treated for 18 h with
945 vehicle, **147** (10 μM) or Rb-11-ca (30 μM) and then metabolically labeled with [^{35}S] for 30 min.
946

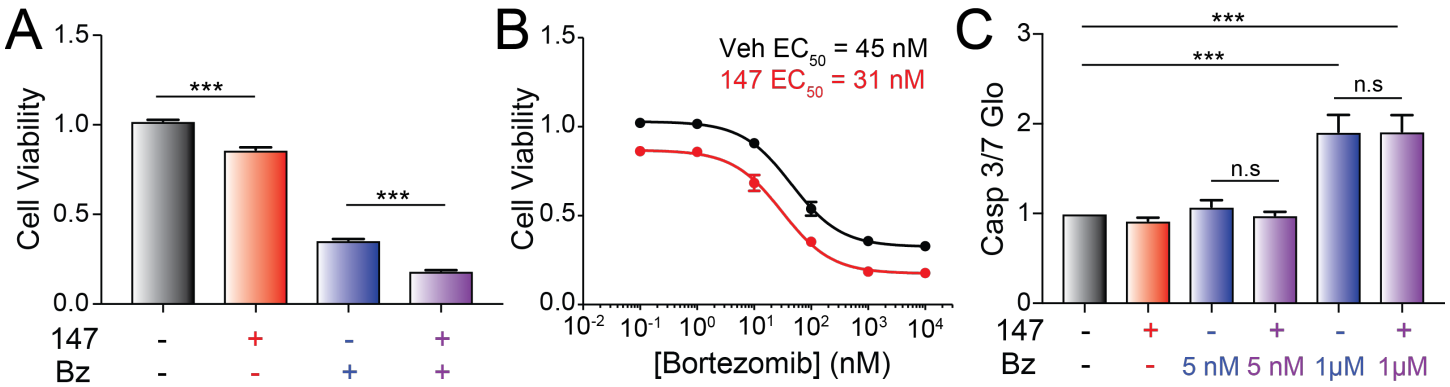

Figure 7. Compound 147 does not influence bortezomib toxicity in ALMC-2 plasma cells

A. Graph showing normalized quantification of viability measured by CellTiter-Glo of ALMC-2 cells treated with vehicle, **147** (10 μM) and/or bortezomib (1 μM) for 24h. Error bars show SEM for n=5 replicates. ***p<0.05 from an unpaired t-test.

B. Graph showing the viability measured by CellTiter-Glo of ALMC-2 cells treated with **147** (10 μM) and/or increasing concentrations of bortezomib (0-10 μM) for 24 h. Error bars show SEM for n=5 replicates.

C. Graph showing normalized caspase 3/7 activation in ALMC-2 cells treated with **147** (10 μM) and/or the indicated concentration of bortezomib (Bz) for 24 h. Error bars show SEM for n=6 replicates across two independent experiments. ***p<0.005 from an unpaired t-test. (n.s), not significant.